Mineralogical Magazine, August 2016, Vol. 80(5), pp. 781–807

OPEN ACCESS

Determination of zeolite-group mineral compositions by electron probe microanalysis

L. S. CAMPBELL[1,*], J. CHARNOCK[1], A. DYER[2], S. HILLIER[3,4], S. CHENERY[5], F. STOPPA[6], C. M. B. HENDERSON[1], R. WALCOTT[7] AND M. RUMSEY[8]

[1] School of Earth, Atmospheric and Environmental Sciences, University of Manchester, Williamson Building, Oxford Road, Manchester M13 9PL, UK
[2] Materials and Physics Research Centre, University of Salford M5 4WT, UK
[3] James Hutton Institute, Craigiebuckler, Aberdeen AB15 8QH, UK
[4] Swedish University of Agricultural Sciences, SLU, Department of Soil & Environment, SE-75007 Uppsala, Sweden
[5] British Geological Survey, Keyworth, Nottingham NG12 5GG, UK
[6] Department of Psychological, Humanistic and Territory Sciences of G.d'Annunzio University Chieti-Pescara, 66100 Chieti, Italy
[7] Department of Natural Sciences, National Museums Scotland, Chambers Street, Edinburgh EH1 1JF, UK
[8] Department of Mineralogy, The Natural History Museum, Cromwell Road, London SW7 5BD, UK

[*Received 31 March 2015; Accepted 22 October 2015; Associate Editor: Katharina Pfaff*]

ABSTRACT

A new protocol for the quantitative determination of zeolite-group mineral compositions by electron probe microanalysis (wavelength-dispersive spectrometry) under ambient conditions, is presented. The method overcomes the most serious challenges for this mineral group, including new confidence in the fundamentally important Si-Al ratio. Development tests were undertaken on a set of natural zeolite candidate reference samples, representing the compositional extremes of Na, K, Cs, Mg, Ca, Sr and Ba zeolites, to demonstrate and assess the extent of beam interaction effects on each oxide component for each mineral. These tests highlight the variability and impact of component mobility due to beam interaction, and show that it can be minimized with recommended operating conditions of 15 kV, 2 nA, a defocused, 20 µm spot size, and element prioritizing with the spectrometer configuration. The protocol represents a pragmatic solution that works, but provides scope for additional optimization where required. Vital to the determination of high-quality results is the attention to careful preparations and the employment of strict criteria for data reduction and quality control, including the monitoring and removal of non-zeolitic contaminants from the data (mainly Fe and clay phases). Essential quality criteria include the zeolite-specific parameters of R value ($Si/(Si+Al+Fe^{3+})$), the 'E%' charge-balance calculation, and the weight percent of non-hydrous total oxides. When these criteria are applied in conjunction with the recommended analytical operating conditions, excellent inter-batch reproducibility is demonstrated. Application of the method to zeolites with complex solid-solution compositions is effective, enabling more precise geochemical discrimination for occurrence-composition studies. Phase validation for the reference set was conducted satisfactorily with the use of X-ray diffraction and laser-ablation inductively-coupled plasma mass spectroscopy.

KEYWORDS: natural zeolite, electron microprobe, analytical protocol, mineral compositions, solid solution.

Introduction

ZEOLITE-group minerals are hydrated aluminium silicates of the alkali and alkaline earth elements, with open framework structures of linked $(Si,Al)O_4$ tetrahedra (Passaglia and Sheppard, 2001; Deer *et al.*,

*E-mail: Linda.Campbell@manchester.ac.uk
DOI: 10.1180/minmag.2016.080.044

2004). They are well known for their properties as ion exchangers and as 'molecular sieves' (Dyer, 1988), and natural zeolites are exploited widely as industrial minerals in applications as diverse as soil amendments, swimming pool filtration, wine making, pharmaceuticals (Daković *et al.*, 2014), and nuclear waste management (Dyer, 2000). In addition to natural varieties, hundreds of synthetic zeolites and similarly-structured materials of other compositions ('zeotypes') have become well established for high-specificity applications in petroleum and material sciences (Čejka *et al.*, 2010).

The scientific value of zeolites in the Earth sciences is found partly in their sensitivity to different temperatures and geochemical environments (Chipera and Apps, 2001), enabling predictive deductions to be made about formation conditions from mineral assemblages and compositions (e.g. Neuhoff *et al.*, 2000; Bish and Ming, 2001; Giampaolo *et al.*, 2008; Campbell *et al.*, 2012; Langella *et al.* 2013; Weisenberger *et al.*, 2014; Cappelletti *et al.*, 2015). This has particular relevance to hydrothermal, surface and diagenetic systems, where mineral compositions can track changing fluid regimes (Hay and Sheppard, 2001; Langella *et al.*, 2001; Utada, 2001, Campbell *et al.*, 2012; Langella *et al.* 2013; Weisenberger *et al.* 2014). Where natural mineral reaction paths involving zeolites are combined with other geological criteria, they have potential value in mineral exploration (Campbell *et al.*, 2012, 2013, 2014), in deepening understanding of global carbon cycling and climate change (Heister *et al.*, 2001; Campbell *et al.*, 2012) and in contributing to the rationalization of volcanic hazard processes (Giampaolo *et al.*, 2008; Bear *et al.*, 2009; Vignaroli *et al.*, 2014). Further, mineral reactions involving zeolites are relevant to studies on the fate of nuclear waste (Wallace *et al.*, 2013). In all these cases, a robust method of mineral analysis is required to achieve full, high quality and reproducible data sets of zeolite mineral compositions, for use in geological and geochemical interpretation based on better understandings of atomic substitutions (Neuhoff and Ruhl, 2006; Gatta *et al.*, 2009). The primary objective of this study therefore, was to generate and validate a robust protocol for the routine determination of zeolite-group mineral compositions by electron probe microanalysis (EPMA, or 'microprobe'). A secondary objective was to select and characterize a set of reference zeolites representative of the compositional extremes of this mineral group, for future quality assurance in analysis.

It is well known that there are severe and inherent problems with the analysis of zeolite-group minerals using micro-beam methods of X-ray generation (Henderson *et al.*, 2014; Weisenberger *et al.*, 2014). Quantitative detection of the resulting characteristic X-rays is either by energy-dispersive spectrometry (EDS), or by wavelength-dispersive spectrometry (WDS). The main problems arise from the interaction of the electron beam with the sample, causing heating (thermal properties of zeolites are reviewed in Bish and Carey, 2001), and diffusive mobility of compositional components in and around the analytical volume, as demonstrated in Kearns and Buse (2012), for alkalis in volcanic glass, and further potentially explained by charge implantation (Cazaux, 2004; Fakhfakh *et al.*, 2010). The mobility includes dehydration and various effects on the light elements, Na, Mg, Al, Si, as indicated in related studies (Line *et al.*, 1995; Morgan and London, 1996, 2005; Vaggelli *et al.*, 1999; Deer *et al.*, 2004; Putnis *et al.*, 2007; Rigby *et al.*, 2008; Weisenberger and Spürgin, 2009; Kearns and Buse, 2012; Henderson *et al.*, 2014; Pearce *et al.*, 2014). These studies, though mostly on glasses and non-zeolitic mineral phases, bear relevance to the EPMA analysis of zeolites. This is because the extra-framework cations in zeolites, especially the lighter alkalis, are very loosely bound in exchangeable sites, with complex crystal-chemical relationships with lattice H_2O and with the Si-Al oxide framework (Passaglia and Sheppard, 2001). Atoms in natural glasses have some level of structural co-ordination (Si-Al tetrahedra, as polymerized 'networks' with interstitial cations which may, or may not, be hydrated), regardless of having no crystal structure, as such. A critical issue for zeolite-group minerals is in the loss of Na with concomitant differential 'grow-in' of Al and Si (as described by Morgan and London, 1996, 2005 for glasses), and the limitation that this places on determination of the Si/Al ratio, which is of fundamental importance in the quantification of zeolite compositions (Passaglia and Sheppard, 2001; Neuhoff and Ruhl, 2006). The general understanding of Al + Si 'grow in' is that as the light and volatile components are driven away from the heated interaction volume (in our case, of the zeolite structure), the apparent, relative concentrations of Si and Al increase. Morgan and London (1996) also explain that the outward migration of Na causes a reduction in the absorption of emitted X-rays from the other elements, and that this effect is greater for Al$K\alpha$ than for Si$K\alpha$ due to relative differences in mass absorption coefficients.

Further, it is possible that dynamic interactions between H_2O and extra-framework cations influence framework bond strengths and angles during dehydration, potentially leading to phase transitions (Wang and Bish, 2012, 2014). Electron beam interaction can also affect the apparent K signal in specific zeolite minerals, notably chabazite, as we report here. Time-dependent intensity (TDI) calculations are referred to by Morgan and London (2005) as a possible way to deal with alkali migration issues in EPMA. However, it is considered that errors introduced through the assumptions and estimates that are needed for this method would probably be much higher than the negligible, measurable errors resulting from element prioritizing in the analysis protocol. The results shown in Test 4 confirm that element prioritizing is a reasonable method, and that TDI is not required. With the advent of field-emission gun (FEG) technology in new-generation microprobes (Merlet and Llovet, 2012, Saunders *et al.*, 2014), it is anticipated that very significant future improvements relating to beam interaction problems will be possible for zeolite analysis, allowing much higher spatial resolution studies to be undertaken.

An additional problem for EDS methods is in the peak overlaps of Si-*K* and Sr-*L* X-ray emission peaks, again precluding the effective determination of Si/Al due to the presence of Sr, which can be an important element in many natural zeolites (Passaglia, 1970; Pekov *et al.*, 2000; Deer *et al.*, 2004; Campbell *et al.*, 2015), and which also requires measurement. In this present study, we address all these problems with tests using a WDS method (non-FEG EPMA, with a 5-spectrometer Cameca SX100 microprobe), on a representative set of candidate reference zeolites. Based on our findings, we present recommended, pragmatic protocols for analysis and data processing for the robust, yet routine, ambient temperature quantification of zeolite compositions by conventional EPMA.

Analytical methods and approach to development

Operating conditions

Initial decisions on the microprobe instrumentation set-up and operating conditions were based on the published literature (Morgan and London, 1996; Giampaolo *et al.*, 1997; Vaggelli *et al.*, 1999; Morgan and London, 2005; Rigby *et al.* 2008; Weisenberger and Spürgin, 2009; Kearns and Buse, 2012; Weisenberger *et al.*, 2014; Henderson *et al.*, 2014; and Danisi *et al.*, 2015). The cryometric method of Kearns and Buse (2012) is acknowledged as a highly effective way of minimizing the heating effect of beam interaction, but it is a specialized technique that is not widely accessible in many EPMA laboratories. Instead, therefore, ambient temperatures were used in the current study, optimizing the other important parameters of beam current, spot size, and order of detection of elements in the spectrometer set-up (see Table 1 for main analyses and Table 2 for X-ray mapping), with the most susceptible elements Na, Al, K, Cs and Ca being analysed first and simultaneously on five separate spectrometers to minimize problems. The beam conditions were first set to 15 kV, 4 nA and 20 µm (defocused), and later set to 2 nA for our established protocol. The selection of an accelerating voltage of 15 kV represents a compromise between limiting the beam penetration depth and corresponding light-element X-ray absorption effects (which increase with increasing kV – see Merlet and Llovet, 2012), and limiting the thermal effect of a higher electron density with a smaller (shallower) volume of interaction at lower kV (Morgan and London, 2005). Nevertheless, the complexity of beam interaction effects on alkali silicate materials as indicated by Cazaux (2004), suggests that there is future scope for examining the effect of varying the kV specifically for zeolites. This is supported by a useful review explaining a number of parameters that are affected by low kV EPMA, but mainly relevant to FEG-EPMA (Merlet and Llovet, 2012).

Tests using each of the other operational configurations in the present study were run on a set of natural zeolites chosen to represent all key compositional ‘end-members’ (See the section on Reference samples and Table 3, described below), and the data were then evaluated for understanding optimal set-up parameters. One of the most important types of test was count-rate monitoring at intervals of 200 ms over 300 s, per element, per sample, as this would reveal the differential extent of sensitivities to beam interaction (see Test 4).

Calibration

Instrument calibration standards for the Manchester Cameca SX100 microprobe relevant to this study are listed in Table 1. These standards, and many others, are employed on a regular basis for routine weekly instrument calibration and used by all analysts. A wider set than listed in Table 1 was further used in the present study with our run file to

TABLE 1. Spectrometer configuration for the WDS analysis of zeolite-group minerals. Operating conditions for the quantitative, 20 μm-defocused, single spot analyses were 2 nA and 15 kV.

Order in analysis cycle	WD Spectrometer	Element	X-ray signal	Detector crystal[§]	Time (s)	Calibration standard (and label)
1st	Sp 1	Cs	Lα	LLIF	20	Cs-glass (csgl)
1st	Sp 2	Ca	Kα	PET	20	Wollastonite (wol)
1st	Sp 3	K	Kα	LPET	20	K-feldspar (ksp)
1st	Sp 4	Al	Kα	TAP	20	Corundum (cor)
1st	Sp 5	Na	Kα	TAP	20	Jadeite (jad)
2nd	Sp 1	Fe	Kα	LLIF	20	Fayalite (fay)
2nd	Sp 2	Ba	Lα	PET	20	Ba-glass (bagl)
2nd	Sp 3	Sr	Lα	LPET	10	Sr-glass (srgl)
2nd	Sp 4	Si	Kα	TAP	20	Wollastonite (wol)
2nd	Sp 5	Mg	Kα	TAP	20	Periclase (per)
3rd	Sp 1	–				
3rd	Sp 2	–				
3rd	Sp 3	*P	Kα	LPET	20	Apatite (apt)
3rd	Sp 4	–				
3rd	Sp 5	* # Rb	Lα	TAP	20	Rb-glass (rbgl)

§LLIF: Lithium fluoride; PET and LPET: Pentaerythritol; TAP: Thallium acid pthalate
#In initial runs, Rb was analysed prior to Mg using Sp5
*P and Rb were only used in the analytical development stages

assess for potential unresolved interferences, and therefore they also serve as 'interference blanks'. The findings are described in Test 1.

Element set-up

The five-spectrometer configuration for our analytical protocol is given in Table 1. Based on the recommendations of Morgan and London (1996, 2005), and on recent studies of natural zeolites (Langella *et al.*, 2013; Weisenberger *et al.*, 2014; Henderson *et al.*, 2014), the priority was to analyse Na and Al first (TAP detectors) with K and Ca (PET detectors), and Cs (LIF) simultaneously, followed immediately by the other elements (Si, Mg, Sr, Ba and Fe). Rubidium was monitored in initial runs, but never detected (limit of detection generally <0.06 wt.% Rb_2O for most zeolites, and 0.21 wt.% Rb_2O for pollucite). Apart from in leucite and clinoptilolite, where minor Fe^{3+} is known in

TABLE 2. Spectrometer configuration for WDS X-ray mapping of zeolite-group minerals. Operating conditions were 20 nA, 15 kV and 5 μm-defocused points. Most arrays were 256 × 256, 200 ms per pixel.

Order in analysis cycle	WD Spectrometer	Element	X-ray signal	Detector crystal[§]	Time (s)
1st	Sp 1	Cs	Lα	LLIF	0.2
1st	Sp 2	Ca	Kα	PET	0.2
1st	Sp 3	K	Kα	LPET	0.2
1st	Sp 4	Al	Kα	TAP	0.2
1st	Sp 5	Na	Kα	TAP	0.2
2nd	Sp 1	Fe	Kα	LLIF	0.2
2nd	Sp 2	Ba	Lα	PET	0.2
2nd	Sp 3	Sr	Lα	LPET	0.2
2nd	Sp 4	Si	Kα	TAP	0.2
2nd	Sp 5	Mg	Kα	TAP	0.2

[§] LLIF: Lithium fluoride; PET and LPET: Pentaerythritol; TAP: Thallium acid pthalate

TABLE 3. Candidate reference zeolites. Further details are given in Supplementary file 1 (deposited at www.minersoc.org/pages/e_journals/dep_mat_mm.html).

Relevant EC*	Mineral name and generic formula[#]	Locality	Source/supplier	Label (this study)	Source label
Na	Natrolite $Na_2[Al_2Si_3O_{10}]\cdot 2H_2O$	Dean Quarry, Cornwall, UK	Dyer	Z01	
	Natrolite $Na_2[Al_2Si_3O_{10}]\cdot 2H_2O$	Dean Quarry, Cornwall, UK	Dyer	fbN	
	Natrolite $Na_2[Al_2Si_3O_{10}]\cdot 2H_2O$	Dean Quarry, Cornwall, UK	Rochelle	Z02	
Na, Ca	Mesolite $Na_2Ca_2[Al_6Si_9O_{30}]\cdot 8H_2O$	Gran Canaria, Canary Islands, Spain	Stoppa	Z03	
Na	Analcime $Na[AlSi_2O_6]\cdot H_2O$	Dean Quarry, Cornwall, UK	Rochelle/Cook	Z04	H425
	Analcime $Na[AlSi_2O_6]\cdot H_2O$	Strada per cima, Mt Vulture, Italy	Stoppa/Campbell	Z06	IT60
K	Leucite $K[AlSi_2O_6]$	Strada per cima, Mt Vulture, Italy	Stoppa/Campbell	Z05	IT60
Cs	Pollucite $Cs_2[Al_2Si_4O_{12}]\cdot H_2O$	Unknown (microprobe standard)	Univ. Manchester	Pol	pol
Ca	Wairakite $Ca[Al_2Si_4O_{12}]\cdot 2H_2O$	Tohi Mine, Shizouka, Honshu, Japan	NHM/Rumsey	Z17	BM 1980,1
	Laumontite $Ca_4[Al_8Si_{16}O_{48}]\cdot 18H_2O$	Poona, Maharashtra, India	NHM/Rumsey	Z18	BM 1975, 339
	Goosecreekite $Ca[Al_2Si_6O_{16}]\cdot 5H_2O$	Maharashtra, India	NHM/Rumsey	Z19	BM 1984, 376
Ba	Edingtonite $Ba[Al_2Si_3O_{10}]\cdot 4H_2O$	Old Kilpatrick, Dumbartonshire, UK	NMS/Walcott	Z12	G.452.10
	Edingtonite $Ba[Al_2Si_3O_{10}]\cdot 4H_2O$	Old Kilpatrick, Dumbartonshire, UK	NMS/Walcott	Z13	G.452.7
	Edingtonite $Ba[Al_2Si_3O_{10}]\cdot 4H_2O$	Ice River, Canada	NHM/Rumsey	Z21	BM 1980,7
Sr, Ba	Brewsterite $(Sr,Ba)_2[Al_4Si_{12}O_{32}]\cdot 10H_2O$	Corantee vein, Strontian, UK	NMS/Walcott	Z14	G.1971.13.1
	Brewsterite $(Sr,Ba)_2[Al_4Si_{12}O_{32}]\cdot 10H_2O$	Corantee vein, Strontian, UK	NMS/Walcott	sbP	G.1971.13.1
Mg, Na, K, Ca	Faujasite $(Mg_{0.5},K,Na,Ca_{0.5})_{3.5}[Al_{3.5}Si_{8.5}O_{24}]\cdot 16H_2O$	Limberg, Sasbach, Kaiserstuhl, Germany	Dyer/Geldart	fbH	6
Ca, Sr, Na, K	Chabazite $(Ca_{0.5},Na,K)_x[Al_xSi_{12-x}O_{24}]\cdot 12H_2O$	Flodigarry, Isle of Skye, UK	Dyer/Geldart	sbZ	
Ca, Na (K)	Levyne $(Ca_{0.5},Na,K)_6[Al_6Si_{12}O_{36}]\cdot 17H_2O$	Moonen Bay, Isle of Skye, UK	Dyer/Geldart	sbW	
K, Na, Ca, Ba	Phillipsite $(K,Na,Ca_{0.5},Ba_{0.5})_x[Al_xSi_{16-x}O_{32}]\cdot 12H_2O$	Matheran, Bombay, Maharashtra, India	NHM/Rumsey	Z20	BM 1988,148

* Extra-framework cation(s) relevant in the context of selections as potential reference minerals. Bold = Most relevant.
\# After Deer *et al.* (2004).
NHM – Natural History Museum, London; NMS – National Museum of Scotland, Edinburgh.

tetrahedral co-ordination (Gatta *et al.*, 2007, for leucite data), Fe in most zeolites is considered to be a contaminant (Passaglia and Sheppard, 2001). It is therefore included in the element list in our analytical protocol as Fe_2O_3 for monitoring of contamination, hence forming one of the decision-criteria for exclusion of low-quality data in our Appendix: Data Reduction and Quality Control Protocol. These checks are necessary in variably-hydrated minerals in which a range of low total oxides can be expected, and they help to minimize uncertainty about the elements that can not be analysed. However, while all analyses in this study are reported on a volatile-free basis with H_2O determined by difference (it can reach to over 20 wt.% in zeolites, Deer *et al.*, 2004), the possibility of minor carbonate or bicarbonate on internal and external mineral surfaces remains (Harjula *et al.*, 1993; Dyer, 2007). Dyer (2007) and Dyer *et al.* (2010) speculated that the unusual ion exchange behaviour of high selectivities of Sr in high-silica zeolites under alkaline conditions could be due to monovalent speciation $[SrX]^+$, (where X- may be OH^- or HCO_3^-). The selectivity is unusual, based on fundamental principles of composition-dependent silicate-solute interactions as discussed in Eisenman (1962) and explained in Colella, (1996), and in Dyer (2000) for zeolites. Hence, low-charge-density (high-Si) zeolites are predicted to show a preference for large, monovalent cations, supporting the notion of the potential presence of anions other than O^{2-}. Carbonate sorption on synthetic zeolite surfaces is discussed in Harjula *et al.* (1993), who demonstrate how the reactive interplay of $NaOH^-$, HCO_3^- and CO_3^{2-} solutes affects the Si-Al framework. For low-Si zeolites, there has been recent interest in the chabazite structure and its affinity for CO_2, in relation to carbon-capture studies using synthetics (Kim *et al.*, 2014; Pham *et al.*, 2014). Thus, while it is difficult to analyse for low concentrations of C routinely by EPMA, its potential presence should be borne in mind in interpretation of compositional data, and its determination by other analytical techniques should be considered (e.g. vibrational spectroscopies for carbonate components). Beryllium, B and Li are also known in some zeolites (Deer *et al.*, 2004), the first two occupying framework tetrahedral sites. However, these rare compositions are not considered in the present study.

Reproducibility

When the optimal operating conditions for zeolite-group minerals were determined, selected reference samples were analysed repeatedly in separate sessions (different days), to monitor inter-batch reproducibility. This was especially of value for the solid-solution compositions (levyne, phillipsite and chabazite), as shown in the results for Test 5. All reference samples were evaluated for homogeneity with the combined use of replicated spot EPMA analyses and of X-ray maps (described in the 'Reference samples' section, below).

Data processing

The raw WDS data were scanned for poor quality analyses on the basis of the following criteria, applied iteratively: (1) Presence of contaminants ($Fe_2O3 > 0.2$ wt.%, and in initial studies, $P_2O_5 >$ Limit of Detection, 'LOD'); (2) application of the '*E*%' error test of Passaglia *et al.* (1970), omitting analyses with *E*% less than –10 or greater than +10; (3) totals of non-volatile oxides outside the range 80–95 wt.%, except for leucite (anhydrous, ideally 100%); and (4) R value, $Si/(\Sigma_{TET})$ (tetrahedral framework cations), outside the ranges listed in table 1 of Passaglia and Sheppard (2001). Once all these criteria were applied, acceptable analyses were then processed for limits of detection, per oxide, per mineral, per session. Deletion of poor data then continued after recalculation of total oxides and *E*%. Calculation of mineral formulae was undertaken according to the conventions set out in Deer *et al.* (2004) based on numbers of framework oxygen atoms specific to each different mineral species. For example, 24 oxygens for chabazite, 20 for edingtonite, 32 for phillipsite, brewsterite and goosecreekite, etc. The H_2O content (wt.%) was determined by difference. Stepwise recommendations using our protocols are given in Appendix 1.

Validation by XRD

Where possible, sub-samples of the reference zeolites used in the EPMA study were independently characterized by X-ray diffraction (XRD). This was primarily for confirmation of mineral phase identification, and the following method was used: Specimens of a few tens of milligrams were hand ground in an agate mortar and pestle for 2 min and the resulting powders sprinkled onto low background silicon single-crystal foil. Specimens were scanned using Ni-filter Cu radiation from 3–70°2θ, in 0.0167° steps counting for 100 s per step using a Panalytical X-pert Pro instrument fitted with an X-celerator position-sensitive detector. Mineral identification was performed using Bruker Diffrac EVA software and comparison to patterns in the Powder Diffraction Files of the International Centre for Diffraction Data: (ICDD PDF-4 2013 database).

Validation by LA-ICP-MS

For compositional validation, there was an opportunity to use major-element data that had been part of a separate, preliminary investigation for trace-element capability using laser ablation inductively-coupled plasma mass spectroscopy (LA-ICP-MS). Samples were analysed using an Agilent 7500 ICP-MS system at the British Geological Survey (Keyworth, UK). This is equipped with a New Wave UP-193 laser ablation system fitted with a 193 nm excimer laser (New Wave Research, Fremont, California, USA), and controlled by New Wave Research-Laser Ablation software. The ablated material is transported in a continuous flow of He to the ICP-MS, where it is vapourized and ionized at 6000 K. Determinations of multi-element mass concentrations were based on calibrations using standard glass NIST612 and an internal ^{44}Ca standard. The method is conveniently capable of near-simultaneous measurement of both major and trace elements, but has limitations in trace-element sensitivities and in analysis volume. Detection limits are proportional to crater volume; to ensure signals above detection limits for some low-abundance elements, craters as large as 100 μm are sometimes required, as in the case of our preliminary trials with zeolites. Another issue is that there are potential interferences of $^{44}Ca^+$ by $^{12}C\text{-}^{16}O\text{-}^{16}O^+$ derived from carbonate or mounting resin, of Ba on the middle rare-earth elements ($^{137}Ba^{16}O^+/^{153}Eu^+$), and mutual doubly charged and polyatomic interferences between Ca and Sr ($^{44}Ca^+/^{88}Sr^{2+}$ and $^{44}Ca\text{-}^{44}Ca/^{88}Sr^{2+}$), limiting potential applications of this particular set-up. All analyses were normalized to the mean SiO_2 wt.% determined by EPMA.

Reference sample selection

One of the key purposes of this study was to compile and characterize a set of reference zeolites for long term use in analytical quality control, as no suitable certified reference materials have been available previously. Whilst there is an abundance of synthetic zeolites available for industrial uses, they are all microcrystalline and hence, unsuitable for the present purpose (Fischer, 2014). The availability of single crystals from natural samples therefore remains as providing the best opportunity for developing sets of reference data. The criteria for selection of our candidate reference minerals of trusted provenance were: (1) representation of compositional end-members by extra-framework Na, K, Cs, Mg, Ca, Sr and Ba; (2) representation of different zeolite structural types; and (3) ideally, a minimum crystal size of ~1 mm^3. All the common extra-framework cations are represented in our candidate reference samples (Table 3 and Supplementary file 1 that has been deposited with the Principal Editor of *Mineralogical Magazine* and is available from www.minersoc.org/pages/e_journals/dep_mat_mm.html). The pollucite for Cs ($Cs_2Al_2Si_4O_{12}.H_2O$), is of unknown provenance, but was available in the set of microprobe calibration standards at Manchester University. Here, we simply report its analysed composition based on our new protocols. Whilst leucite for K is now formally classified with the zeolites, it has limited value as a reference material for zeolitic K because it is not hydrated (see Henderson *et al.*, 1998, for discussion of the crystal chemistry of the leucite-pollucite-wairakite structure type). Henderson *et al.* (2014) showed that the $NaAlSi_2O_6.H_2O$ component of leucites can be up to a maximum of 4 wt.%. Nevertheless, the reasonably consistent formula and lower Si:Al of leucite than of K-feldspar renders it useful in conjunction with the solid solutions levyne (sbW), chabazite (sbZ) and phillipsite (Z20). The faujasite (fbH for Mg-reference) and brewsterite (Z14 and sbP for Sr-reference), similarly, are solid solutions but necessarily part of the reference set due to the absence of pure Mg and Sr end-member zeolites in nature. The inclusion of natural zeolite minerals which display solid-solution ranges was considered important as these minerals are reported widely in occurrence studies and have considerable value in geochemical discrimination when used in conjunction with paragenesis information (e.g. Heister *et al.*, 2001; Weisenberger and Spürgin, 2009; Weisenberger *et al.*, 2012, 2014; Langella *et al.*, 2013; Campbell *et al.*, 2015; Cappelletti *et al.*, 2015). The solid-solution samples additionally have value in monitoring reproducibility (see Test 5). A future objective is to acquire and characterize a suitable heulandite or clinoptilolite reference sample, representing high-Si zeolites that display complex solid-solution systematics. Clinoptilolite deposits occur abundantly and are economically important as industrial minerals. Examples of geologically-relevant structural-type differences in the reference set are provided by natrolite and analcime for Na end-members, and wairakite, laumontite and goosecreekite for Ca end-members.

Results

Reference sample characterization

Details of the selected candidate reference samples and their sources are given in Table 3 and Supplementary file 1 (Supplementary files 1–4 are deposited at www.minersoc.org/pages/e_journals/dept_mat_mm.html), and diagrams of their mounted positions in the polished sections are provided in Supplementary file 2, for potential long-term reference. Optical and electron microscopic images were collected for navigation and quality evaluation purposes, and X-ray maps were collected to assess compositional homogeneity. All of these images are compiled in Supplementary file 3. The phillipsite (Z20) and one of the brewsterites (Z14) did not display adequate compositional homogeneity for full use as secondary standards, but in the absence of any other Sr-rich zeolite, the brewsterite nevertheless has value as a basic-level reference material, as discussed above, and in the analysis development tests of the present study (below).

Averaged, optimum analyses for each mineral determined using our final, recommended protocol, are shown in Table 4, but the full set of EPMA analyses based on a variety of test parameters are given in Supplementary file 4, with limits of detection. The detail and pattern of results for each development test are explained below. Where available, analyses are compared with those from previously published data, as detailed in Deer *et al.* (2004) and in other more recent publications. Note the excellent ‘error test’ (*E*%, Passaglia, 1970) results and low variances of the new data in the summary table (Table 4). Passaglia (1970) recognized the scope of a simple arithmetic test for zeolitic analytical quality, by using the mineralogical constraint of the charge equivalence of Al^{3+} (and the associated anionic excess in the $[Si,Al]O_4$ framework), with the sum of the charges of the extra-framework cations. Thus, an *E*% value of zero represents full stoichiometry (excluding H_2O). The general guidance for acceptable analyses is that they should fall within the *E*% range –10 to +10%, but even better, within the range –7 to +7%. In Table 4, most data fall within –2 to +2%, with only natrolite Z01 outside this very high quality range at –5.32% and a ‘replacement’, or ‘X-type’ analcime (Giampaolo and Lombardi, 1994; Henderson *et al.*, 2014) at +7.5%. Error test results in Supplementary file 4 should be read in conjunction with the appropriate descriptions of the development tests, explained fully, below.

Reference sample validation

XRD data

Mineral phase identifications are shown in Fig. 1, with spectral traces in colour superimposed onto the ideal (ICDD) peak positions and intensities in grey/black. The results serve as verification for all phases determined this way.

LA-ICP-MS data

In Table 5, averaged LA-ICP-MS results for the major elements are presented, with normalization to the mean wt.% SiO_2 as determined by EPMA. There is excellent agreement of results for three candidate reference materials natrolite (fbN), brewsterite (sbP) and levyne (sbW), except for Ca (extrapolated from ^{42}Ca) in the LA-ICP-MS data, relative to the microprobe data (Table 4 and Supplementary file 4).

Development test results and discussion

Test 1: X-ray interferences

Following an evaluation of potential peak overlaps using ‘*Virtual WDS*’ software, and adjusting background positions and spectrometer choices accordingly, this first test examined the quality of ‘blank’ runs acquired on the calibration standards. All blank runs provided satisfactorily low blanks for zeolite-relevant major elements. The apparent 0.5 ± 0.15 wt.% Al_2O_3 seen for the barite standard is unexplained but assumed to be a contamination issue rather than an interference, as no similar signal was found for the benitoite ($BaTiSi_3O_9$), the anhydrite or the celestine standards (relating to Ba and S components respectively). The potential Ti-Ba X-ray interference was tested with the rutile standard satisfactorily. In our protocol, Ba-glass was used as the calibration standard for Ba (Table 1). Although Cs-glass was used as the calibration standard for Cs, a pollucite standard of unknown source was also available, and it was decided that this could serve as the Cs end-member reference mineral for the present study. Analyses of the pollucite standard were therefore collected,

TABLE 4. Summary EPMA data for the candidate reference zeolites determined with the final analytical and data processing protocols (Appendix 1). A full set of individual analyses with detection limits is given in Supplementary file 4.

Mineral	Natrolite						Mesolite		Analcime				Leucite		Pollucite	
Label	Z01		fbN		Z02		Z03		Z04		Z06		Z05		Pol	
No. of analyses	5		5		5		5		8		5		8		8	
	Mean	s^2	Mean	s^2	Mean	s^2	Mean	s^2	Mean	s^2	Mean	s^2	Mean	s^2	Mean	s^2
SiO_2	46.49	0.30	47.02	0.05	47.51	0.02	45.63	0.04	53.74	0.47	53.38	0.14	53.69	0.73	43.47	0.51
Al_2O_3	26.34	0.11	26.48	0.04	27.07	0.02	25.38	0.07	22.68	0.15	23.16	0.03	22.75	0.06	15.38	0.06
Fe_2O_3													0.260	0.001		
MgO																
CaO					0.027		11.85	0.19			0.466	0.005				
SrO	0.086								0.027	0.002	0.052	0.005				
BaO									0.039	0.012			0.029	0.007		
Na_2O	16.89	0.11	16.44	0.19	16.49	0.11	2.60	0.06	14.05	0.27	12.55	0.09	0.825	0.004	1.929	0.029
K_2O													20.04	0.04		
Cs_2O	0.237														33.29	0.47
Total	89.782	0.656	89.943	0.547	91.075	0.131	85.462	0.062	90.530	2.453	89.612	0.216	97.595	1.428	94.366	1.283
H_2O by difference	10.22		10.06		8.92		14.54		9.47		10.39		2.40		5.63	
Number of cations on the basis of framework oxygens specific to each mineral																
O	80		80		80		80		96		96		96		96	
Si	23.83	0.020	23.98	0.005	23.91	0.014	24.09	0.005	31.97	0.017	31.85	0.027	31.91	0.011	33.68	0.026
Al	15.91	0.027	15.91	0.004	16.06	0.004	15.79	0.018	15.90	0.014	16.28	0.012	15.94	0.014	14.04	0.025
Fe3+													0.1160	0.0002		
∑ T	39.739	0.010	39.893	0.008	39.968	0.007	39.877	0.021	47.868	0.007	48.125	0.005	47.963	0.002	47.722	0.016
Mg																
Ca					0.003	<0.001	6.705	0.063			0.298	0.002				
Sr	0.0048	0.0001							0.0120	0.0003	0.0160	0.0005				
Ba									0.0100	0.0008			0.0070	0.0004		
Na	16.790	0.083	16.254	0.122	16.085	0.076	2.661	0.058	16.192	0.135	14.518	0.128	0.951	0.005	2.898	0.059
K													15.1965	0.0140		
Cs	0.0096	0.0005													11.002	0.072
∑ EC	16.805	0.091	16.254	0.122	16.088	0.077	9.366	0.064	16.214	0.146	14.832	0.097	16.154	0.019	13.899	0.110
R = Si/(Si + Al)	0.600		0.601		0.598		0.604		0.668		0.662		0.667		0.706	
E% (Passaglia 1970)	−5.32		−2.06		−0.19		−1.69		−2.03		7.50		−1.37		1.09	

TABLE 4. (*Contd*).

Mineral	Wairakite		Laumontite		Goosecreekite		Edingtonite							
Label	Z17		Z18		Z19		Z12		Z13		$Z21_{core}$		$Z21_{rim}$	
No. of analyses	7		9		9		5		5		12		3	
	Mean	s^2	Mean	s^2	Mean	s^2	Mean	s^2	Mean	s^2	Mean	s^2	Mean	s^2
SiO_2	54.13	0.35	52.69	0.25	58.17	0.34	38.54	0.49	38.52	0.19	36.34	0.35	37.38	0.16
Al_2O_3	22.72	0.03	21.66	0.10	16.67	0.07	20.66	0.05	20.47	0.06	20.42	0.07	20.07	0.20
Fe_2O_3														
MgO														
CaO	12.58	0.10	12.04	0.11	9.21	0.04					0.018	0.002		
SrO			0.018	0.003									0.075	0.017
BaO							30.78	0.27	30.10	0.64	31.01	1.44	29.47	1.47
Na_2O	0.018	0.002	0.036	0.005	0.147	<0.001					0.028	0.004		
K_2O			0.049	0.002	0.152	<0.001	0.462	0.001	0.478	0.020	0.205	0.061	0.698	0.065
Cs_2O			0.017	0.003										
Total	89.450	0.509	86.509	0.861	84.235	0.667	90.434	0.608	89.562	0.474	88.020	1.604	87.694	1.299
H_2O by difference	10.55		13.49		15.77		9.57		10.44		11.98		12.31	
Number of cations on the basis of framework oxygens specific to each mineral														
O	96		48		32		20		20		20		20	
Si	32.05	0.032	16.13	0.002	11.94	0.002	6.10	0.003	6.13	<0.001	5.99	0.003	6.10	0.007
Al	15.85	0.019	7.81	0.005	4.03	0.003	3.86	0.005	3.84	<0.001	3.97	0.003	3.86	0.005
Fe3+														
$\sum$ T	47.902	0.005	23.943	0.004	15.968	0.001	9.960	0.001	9.973	0.001	9.958	0.001	9.963	0.001
Mg														
Ca	7.977	0.035	3.948	0.009	2.024	0.001					0.0033	0.0001		
Sr			0.0033	0.0001									0.0069	0.0001
Ba							1.9100	0.0011	1.8776	0.0035	2.0030	0.0056	1.8844	0.0049
Na	0.0206	0.0030	0.0213	0.0018	0.0129	0.0007					0.0088	0.0004		
K			0.0189	0.0002	0.0397	<0.0001	0.0932	<0.0001	0.0964	0.0008	0.0430	0.0027	0.1453	0.0029
Cs			0.0022	<0.0001										
$\sum$ EC	7.998	0.023	3.994	0.012	2.077	0.002	2.003	0.001	1.974	0.001	2.058	0.002	2.037	0.001
$R = Si/(Si + Al)$	0.669		0.674		0.748		0.613		0.615		0.602		0.612	
E% (Passaglia 1970)	−0.73		−1.58		−1.67		−1.41		−0.23		−2.33		−1.68	

TABLE 4. (*Contd*).

Mineral	Brewsterite				Faujasite		Chabazite		Levyne		Phillipsite	
Label	Z14		sbP		fbH		sbZ		sbW		Z20	
No. of analyses	7		11		5		36		25		36	
	Mean	s^2	Mean	s^2	Mean	s^2	Mean	s^2	Mean	s^2	Mean	s^2
SiO_2	52.03	1.41	51.50	1.29	57.62	0.20	55.01	1.46	49.08	0.45	47.41	1.02
Al_2O_3	15.21	0.18	15.26	0.09	19.19	0.01	19.74	0.16	23.25	0.11	22.19	0.53
Fe_2O_3												
MgO					2.68	0.01	0.025	0.004			0.075	0.051
CaO	0.023	0.004			3.30	0.02	9.11	0.10	10.01	0.12	8.32	0.15
SrO	11.36	0.27	10.96	0.31	0.075	0.028	0.031	0.008	0.143	0.043	0.019	0.004
BaO	5.83	0.37	5.63	0.16	0.047	0.011	0.050	0.011			0.025	0.007
Na_2O	0.072	0.015	0.253	0.012	2.98	0.01	0.97	0.02	2.10	0.08	0.81	0.04
K_2O	0.078	0.002	0.101	<0.001	0.201	0.001	0.93	0.01	0.30	0.01	4.94	0.52
Cs_2O							0.008	0.001	0.020	0.005		
Total	84.605	2.178	83.715	1.177	86.100	0.321	85.835	2.194	84.909	0.843	83.800	2.862
H_2O by difference	15.39		16.29		13.90		14.16		15.09		16.20	
Number of cations on the basis of framework oxygens specific to each mineral												
O	32		32		24		24		36		32	
Si	11.87	0.008	11.85	0.007	10.98	0.001	8.44	0.003	11.59	0.005	10.30	0.015
Al	4.09	0.007	4.14	0.008	4.31	0.001	3.57	0.002	6.47	0.006	5.68	0.021
Fe3+												
$\sum$ T	15.964	0.002	15.990	0.003	15.284	0.001	12.009	0.001	18.060	0.003	15.989	0.004
Mg					0.7608	0.0005	0.0057	0.0002			0.0241	0.0053
Ca	0.0056	0.0002			0.6737	0.0009	1.4976	0.0028	2.5332	0.0081	1.9383	0.0079
Sr	1.5030	0.0026	1.4624	0.0058	0.0084	0.0004	0.0027	0.0001	0.0543	0.0003	0.0024	0.0001
Ba	0.5219	0.0035	0.5081	0.0015	0.0034	0.0001	0.0011				0.0022	0.0001
Na	0.0328	0.0031	0.1136	0.0024	1.1010	0.0019	0.2876	0.0023	0.9611	0.0162	0.3404	0.0070
K	0.0227	0.0001	0.0297		0.0488	0.0001	0.1814	0.0006	0.0901	0.0006	1.3700	0.0375
Cs							0.0005		0.0255			
$\sum$ EC	2.086	0.008	2.114	0.012	2.596	0.003	1.977	0.007	3.606	0.020	3.677	0.021
$R = Si/(Si + Al)$	0.744		0.741		0.718		0.703		0.642		0.644	
E% (Passaglia 1970)	−0.54		1.54		6.60		2.57		5.181		0.82	

s^2 is the sample variance where s is the standard deviation of the mean.

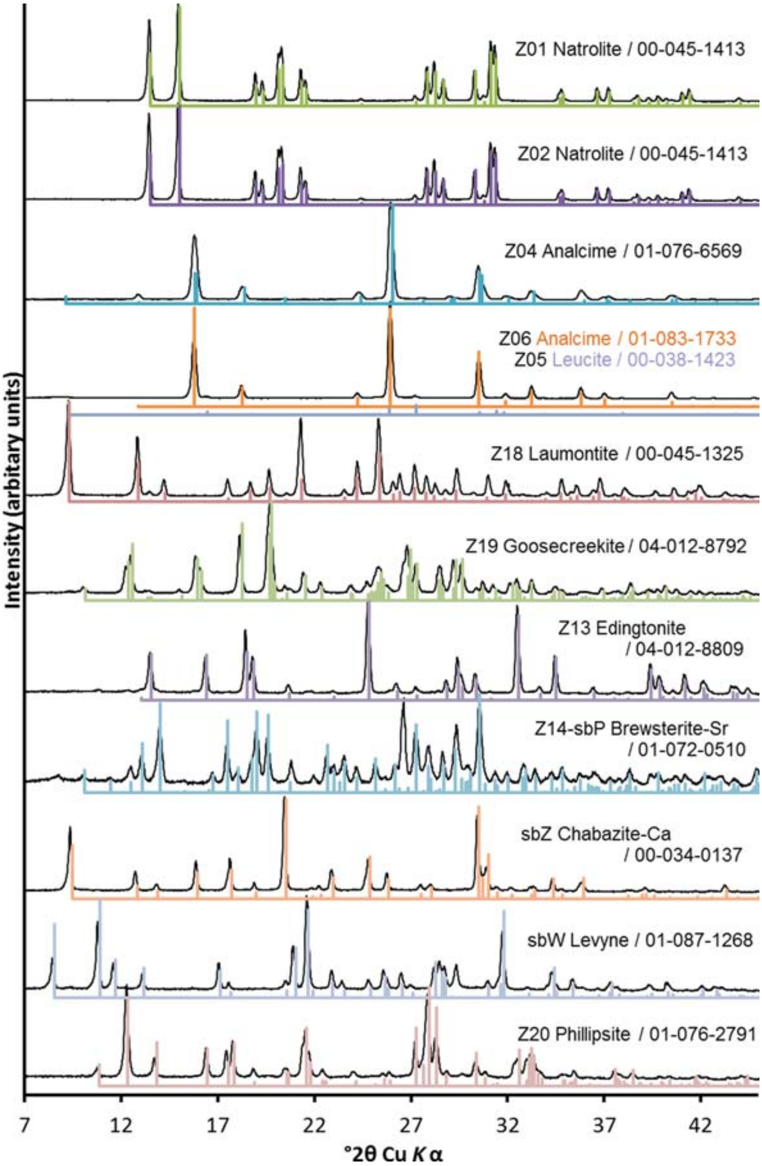

FIG. 1. X-ray diffraction validation data for selected reference samples. The sample patterns are shown in black, and ICDD Powder Diffraction File (PDF) data, in colour. Card references for PDF data are listed with the mineral labels on the figure. Minor impurities of quartz, feldspar and mica were noted for brewsterite (sbP and Z14), and of calcite and chabazite for levyne (sbW).

and presented with all the other results in Table 4 and Supplementary file 4.

Test 2: Effects of beam interaction on basic reproducibility for different minerals.

In this test, multiple analyses were undertaken for a single spot, using a defocused beam of 20 µm, on different minerals. Operating conditions were 4 nA and 15 kV, and two test minerals were used; natrolite Z01 and mesolite Z03. For comparison, similar data for the albite and jadeite standards

TABLE 5. Comparative major element analyses determined by LA-ICP-MS, 100 µm craters. All oxides left blank were undetected at <<0.001 wt.%.

Mineral	Natrolite		Brewsterite		Levyne	
Label	fbN		sbP		sbW	
No. of analyses	5		6		3	
	Mean	s^2	Mean	s^2	Mean	s^2
SiO_2	47.022	<0.001	51.504	<0.001	49.080	<0.001
Al_2O_3	26.677	0.232	14.733	1.447	22.324	7.127
Fe_2O_3						
MgO						
CaO	0.009	<0.001	0.309	0.001	8.713	0.794
SrO			10.630	1.191	0.243	0.002
BaO			4.593	0.226	0.001	<0.001
Na_2O	15.877	0.270	0.103	0.010	2.804	0.015
K_2O			0.062	<0.001	0.249	0.001
Cs_2O						
Total	89.585	0.932	81.936	5.879	83.415	12.898
H_2O by difference	10.415		18.064		16.585	
Number of cations on the basis of framework oxygens specific to each mineral						
O	80		32		36	
Si	24.02	0.04	11.99	0.06	11.79	0.21
Al	16.06	0.03	4.04	0.06	6.30	0.28
Fe3+						
$\sum$ T	40.082	0.006	16.029	0.005	18.094	0.005
Mg					0.0004	<0.0001
Ca	0.005	<0.001	0.077	<0.001	2.2368	0.0219
Sr			1.4331	0.0161	0.0338	<0.0001
Ba			0.4186	0.0016	0.0001	<0.0001
Na	15.722	0.155	0.046	0.002	1.3062	0.0059
K			0.0185	<0.0001	0.0763	<0.0001
Cs						
$\sum$ EC	15.727	0.156	1.994	0.026	3.654	0.011
$R = Si/(Si + Al)$	0.599	<0.001	0.748	<0.001	0.652	0.001
E% (Passaglia, 1970)	2.12		3.26		6.24	

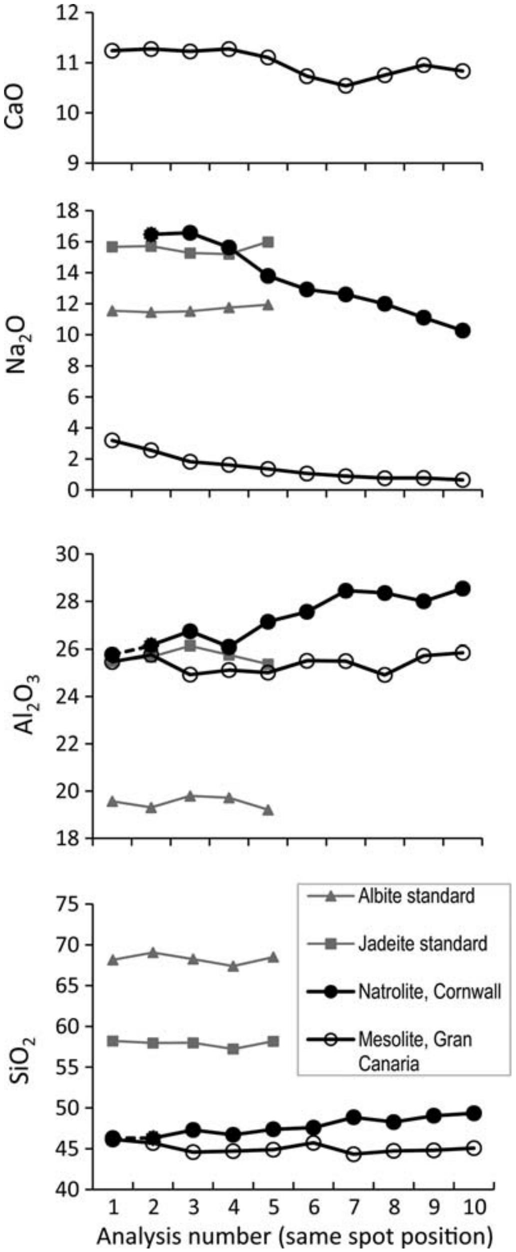

FIG. 2. Test 2: Initial beam interaction tests on natrolite and mesolite, based on repeated analyses on single spots. Jadeite and albite were included for comparison.

(non-hydrated silicates) were obtained. Figure 2 shows the change in apparent oxide wt.% for successive analyses on the same spot. The greatest changes with time are seen for Na_2O and Al_2O_3 in natrolite after the fourth analysis, but steady and immediate losses of Na_2O are seen for mesolite. SiO_2 is generally stable except in natrolite where a small but perceptible change is apparent in the later analyses. These initial observations are consistent with many previous reports of Na loss and Al + Si 'grow in', in hydrous, alkali aluminosilicate glasses, as reported by Morgan and London (1996, 2005). Potential explanations, including heat-driven diffusion (Kearns and Buse, 2012), have been outlined in our introductory paragraphs. Therefore, in consideration of the evidence outlined above for differential effects of beam interaction specific to different elements and different phases, further element-specific and mineral-specific tests were conducted, as follows.

Test 3: Effect of beam current

Adhering to a beam current of <5 nA, based on the findings of Morgan and London (1996), the third set of tests compare analyses determined at 4 nA with those determined at 2 nA, for ten separate reference minerals: leucite, analcime (2), natrolite (3), mesolite, edingtonite (2) and brewsterite; Supplementary file 4. In Fig. 3*a–c*, it can be seen that the 2 nA populations for leucite, X-type analcime (Z06) and mesolite tend to perform better in terms of stoichiometry (based on the *E*% and on total wt.% oxides), than the 4 nA populations, but that for H-type analcime (Z04), there was no difference with current (2 *vs.* 4 nA). For analcimes, a greater influence on the quality of the analysis is in the crystallization history and apparent susceptibility to factors controlling permeability within the crystal. The H-type analcime (Z04) from Dean Quarry (Lizard Complex, Cornwall, UK) is from a pegmatitic/hydrothermal vein, presumably crystallizing directly from a fluid. The analyses display excellent stoichiometry, with H_2O in the range 7–12 wt.%. In contrast, the X-type analcime (Z06) from Mt. Vulture (southern Italy), occurs enclosing leucite (Z05) in an altered pyroclastic deposit, and it crystallized by a replacement mechanism expressed by the well-known ion exchange reaction accompanied by hydration:

$$\underset{\text{Leucite}}{K[AlSi_2O_6]}+Na^{+}+H_2O\Rightarrow \underset{\text{Analcime}}{Na[AlSi_2O_6]\cdot H_2O}+K^{+}$$

These X-type analcimes are commonly reported as being depleted in apparent Na content, and additionally display lower *R* values and extreme

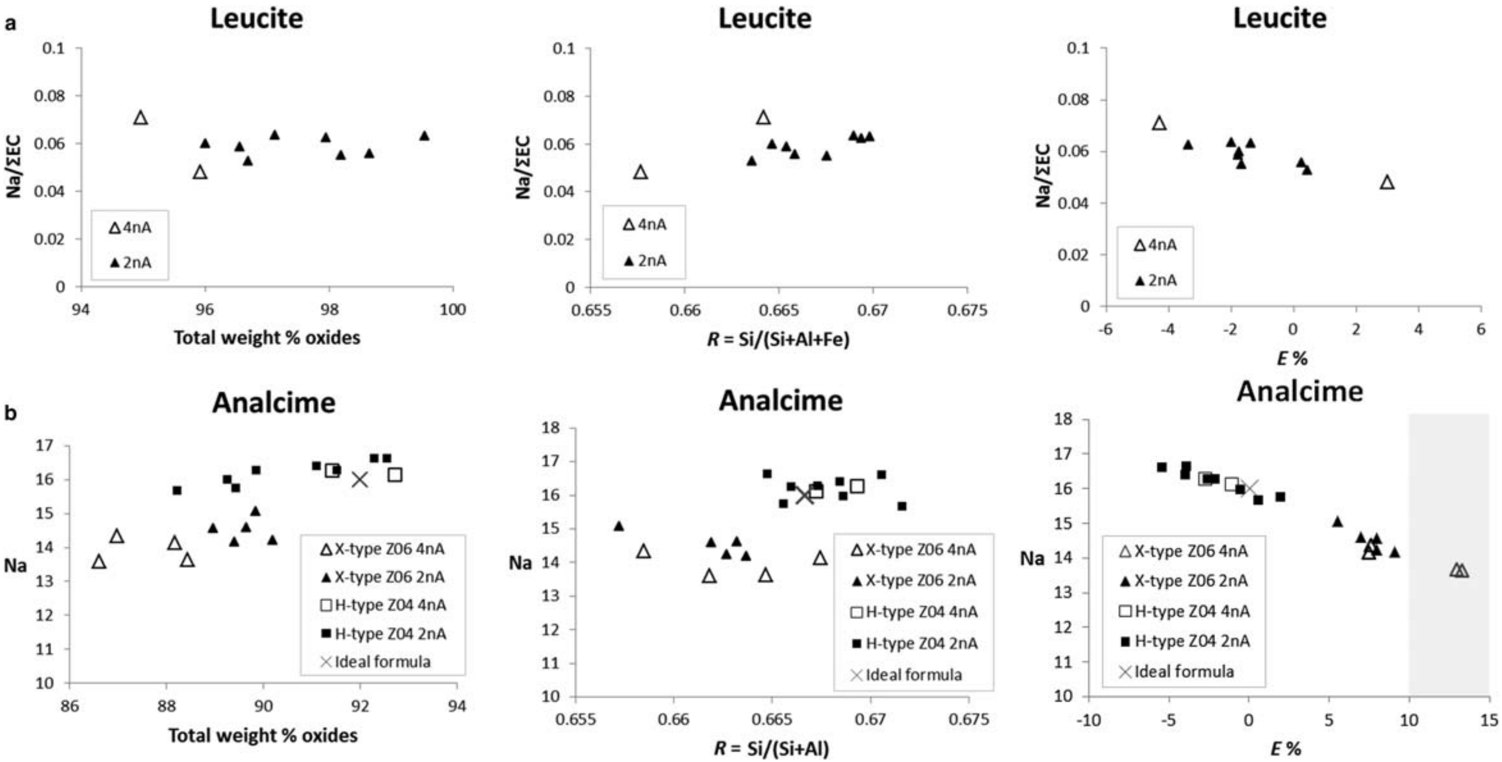

FIG. 3. Test 3: Effect of beam current on analyses of different reference zeolites. Total wt.% oxides exclude H_2O. $\sum$EC = sum of extraframework cations. Areas outside of the acceptable range of *E*% (Passaglia, 1970), are shaded.

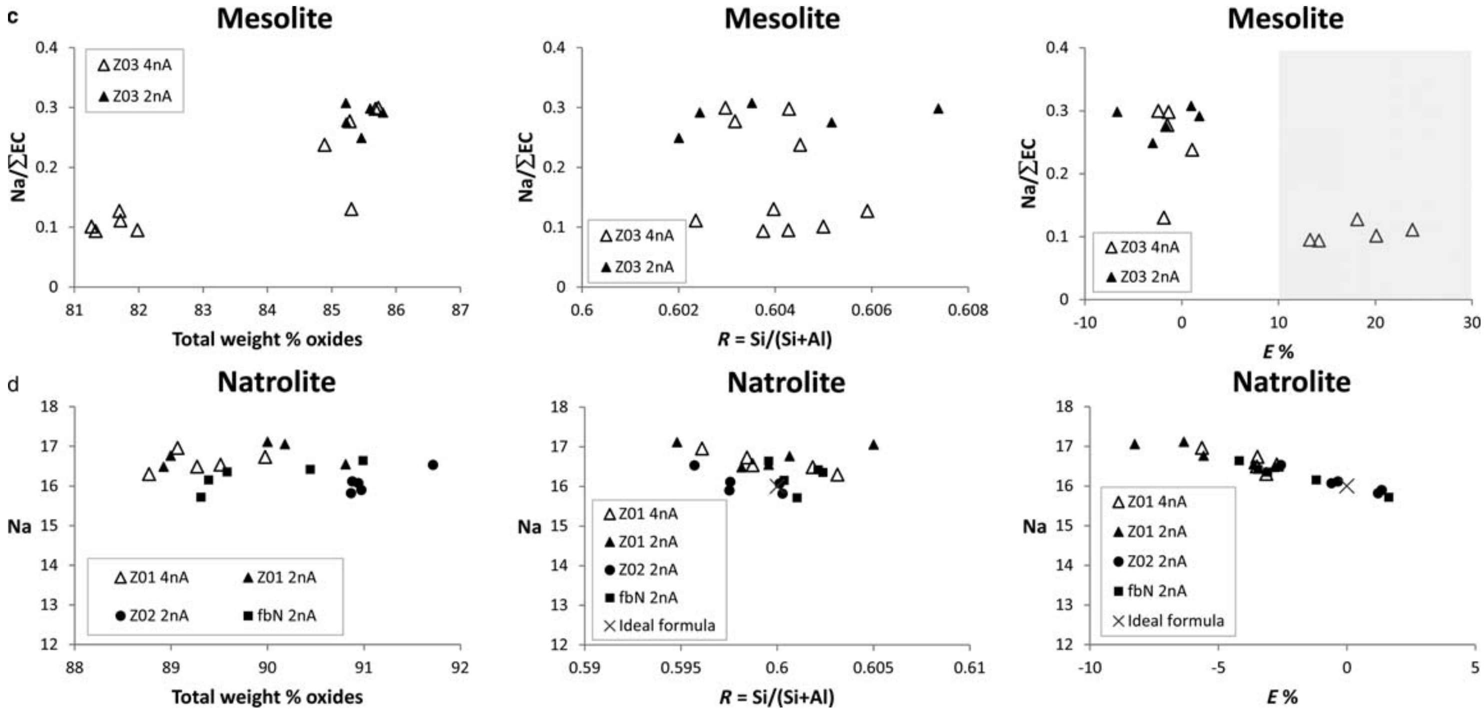

FIG. 3. Continued

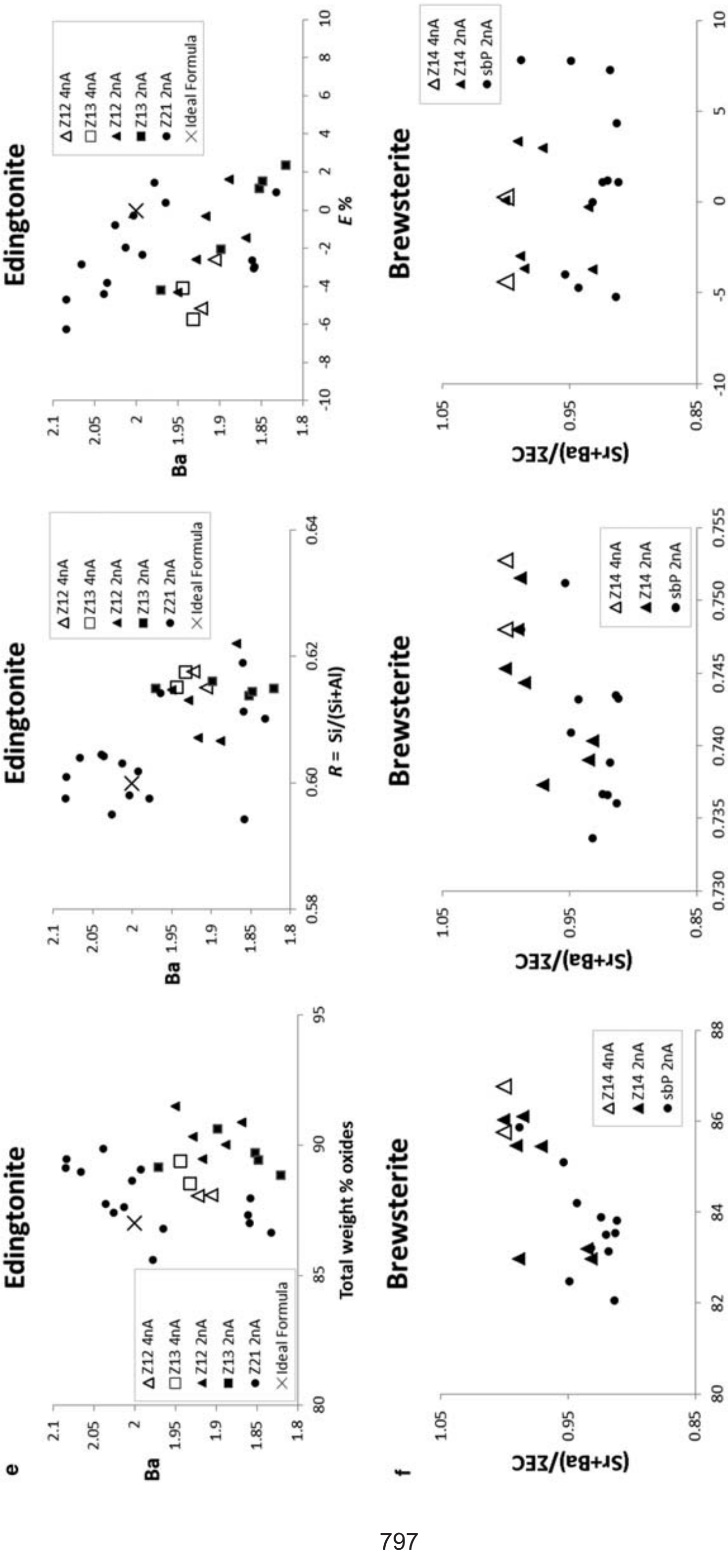

FIG. 3. Continued

E% values than for an ideal analcime (Deer *et al.*, 2004). X-type analcimes as pseudomorphs after leucite, tend to be very fine-grained and polycrystalline, giving a high surface area promoting mobility of volatiles. They contrast the single crystal, vitreous appearance of H-type (hydrothermal) and I-type primary (igneous/magmatic) analcimes (Giampaolo and Lombardi, 1994, Putnis *et al.*, 2007; Henderson *et al.*, 2014). Several reasons for Na-depletion in X-type, beam-affected (dehydrated) analcimes have been discussed previously, and include crystal defects, framework volume increase with fracture development, and H_2O-Na mobility. Additionally, we suggest that the reactive expulsion of trace elements from leucite, possibly remaining *in situ* as micro/nano secondary-phase inclusions in the analcime product, causes further enhancement of the overall permeability, for rapid loss of volatiles on heating (beam interaction). The interface zone in the X-ray maps of the leucite-analcime pair (Supplementary file 3), showing marginally elevated Mg (probably occurring as smectite) is consistent with this, and with the replacement mechanism of dissolution-reprecipitation proposed by Putnis *et al.* (2007). Neither K nor Ca were detected in Z06 (Supplementary file 4, confirmed with X-ray maps of the leucite-analcime pair, Z05 and Z06, Supplementary file 3), indicating a complete absence of potential residual K that might have been derived from the primary leucite. (The apparent trace-Ca in the Z06 map is likely to be a background-matrix artefact, and the traces of leucite in the XRD data for Z06 are due to the paired co-occurrence of the two separate phases and practicalities of complete separation prior to powdering for analysis).

Natrolite and edingtonite displayed no differences in analytical quality due to 2 nA *vs.* 4 nA beam conditions (Fig. 3*d*,*e*).

For Si:Al in all phases studied, the effect of beam current (2 and 4 nA) appears to be minimal or absent, except for where systematic coupled substitutions involving alkalis as seen in brewsterite (Fig. 3*f*), suggest a potential influence. However, only two points of data collected with the 4 nA condition were accepted with our processing protocol, and these happened to display full occupancy of the EC sites by Sr^{2+} and Ba^{2+} alone. Nevertheless, the positive correlation of total oxides with the sum of Sr and Ba (and therefore, of alkali content and H_2O) in the 2 nA brewsterite data, is suggestive of a preferred crystallographic association of H_2O with the alkalis over M^{2+}, potentially leading to dehydration-coupled alkali losses if higher currents were used.

Test 4: Count-rate stability

The extent and analytical impact of beam-interaction susceptibility in different zeolite minerals was investigated by count-rate monitoring tests, per sample, per element, against time at a fixed current of 2 nA. The spectrometer-element configurations were identical to those used for the main analysis run-file (Table 1). The sampling rate was every 0.2 s over a period of 300 s. Spectrometers were run simultaneously where possible, but fresh spot positions were selected when it was necessary to change spectrometer configurations for different elements in these tests. Figure 4 shows selected count rate profiles for reference sample minerals, by element. Signal stability is indicated by a near-horizontal profile, as demonstrated by the Dean Quarry natrolite (Z01) between 0 and 1800 s. In addition to the second-by-second random fluctuations in count rates, most profiles show minor, longer-period fluctuations over several seconds or tens of seconds, but these are generally of lower magnitude than the second-by-second fluctuations, and are probably related to subtle instrument sensitivities to the immediate beam-environment.

Deviations from horizontal profiles that are not accounted for in the above rationale are examined further. Analcime Z06 (X-type) from Mt. Vulture, Italy, displays a marked decrease in count rate for Na (~50%), and a minor increase for Si over the course of 300 s. This pattern, typical of previous descriptions of Na-loss, is not seen in analcime Z04 (H-type) from Dean Quarry, Cornwall, UK. We again account for the differences for this phase by consideration of the beam interaction issues as discussed for Tests 2 and 3, but additionally, the XRD data of Fig. 1 demonstrate crystal structure differences; X-type Z06 is cubic *Ia*3*d* or orthorhombic *Ibca*, whereas H-type Z04 is possibly monoclinic, based on a cubic *Ia*3*d* pseudocell. Analcime is known to crystallize in as many as 5 different crystal systems (Deer *et al.*, 2004). The higher surface area of analcime Z06 also potentially increases its susceptibility to CO_2 sorption from the atmosphere, affecting the overall reactive potential of this Na-rich mineral in alkaline conditions, including framework dissolution (Harjula *et al.*, 1993). Putnis *et al.* (2007) further show that X-type analcimes derived from leucite might undergo replacement processes that are more complex than simple ion exchange. Their evidence is based

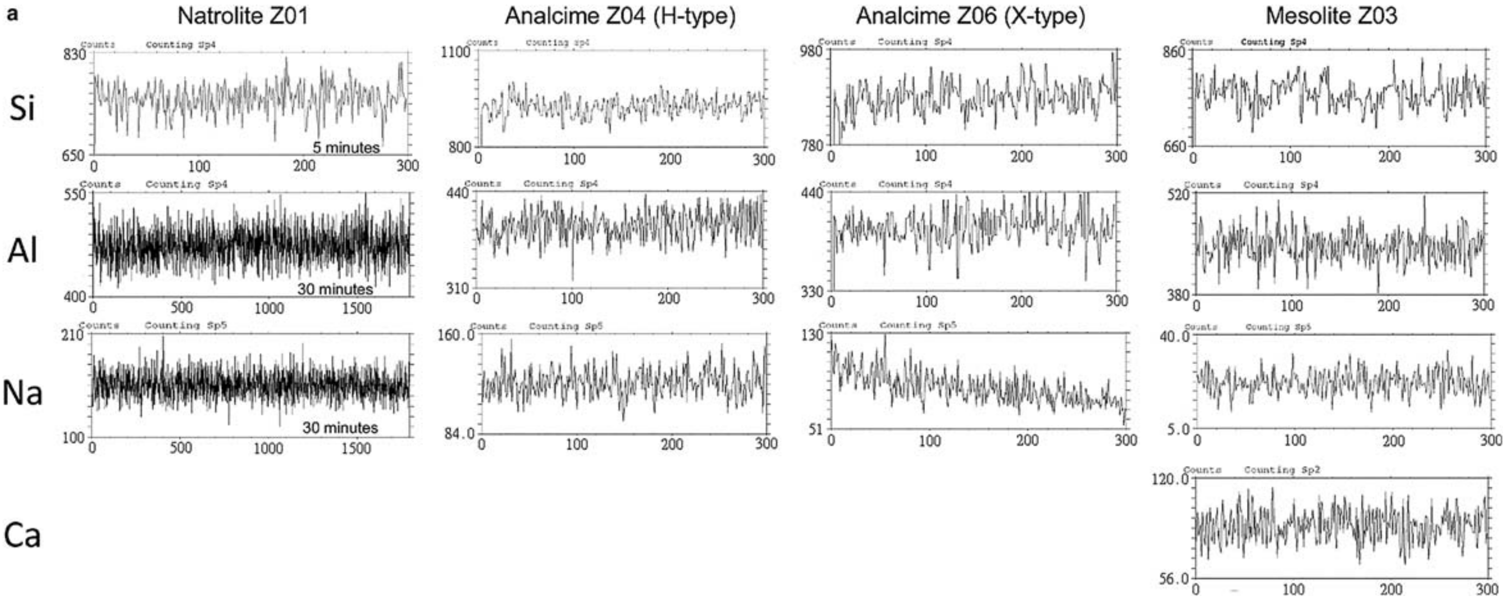

FIG. 4. (*a* above and *b* next page). Test 4: Selected count rate profiles per element per reference zeolite, collected over 300 s (and 1800 s for natrolite, Z01) using a 2 nA, defocused 20 μm beam. The count-sampling interval was every 200 ms. All other reference samples displayed steady, horizontal profiles for every major element in their respective mineral formulae. For clarity only the upper and lower x-axis figures are given.

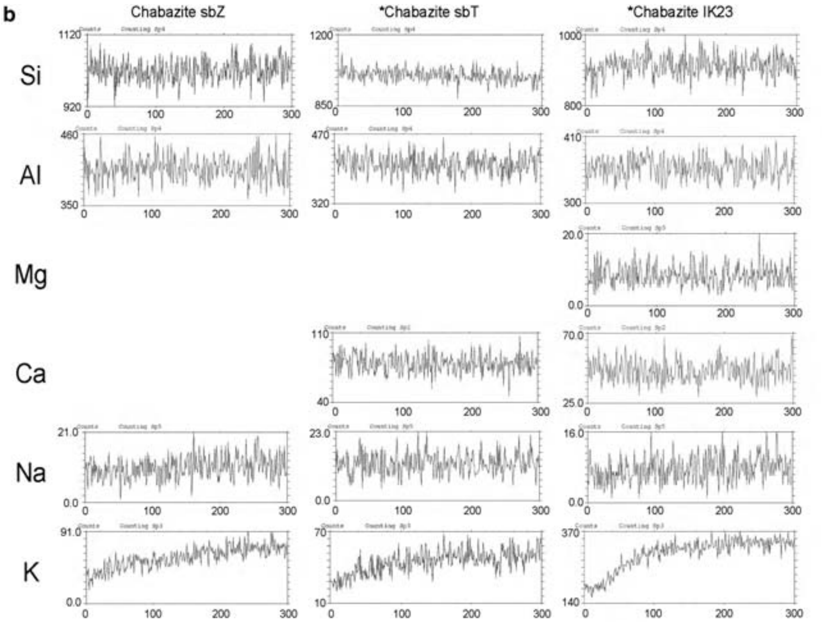

* Chabazites sbT (Skye, UK) and IK23 (Vico, Italy) are part of ongoing studies, illustrated here as replicates for the K response

FIG. 4. Continued

on experiments using ^{18}O water, indicating the involvement of framework-O exchange in the reaction. Other reference samples in the present study displaying cumulative loss of light elements include mesolite (Z03) losing Na and Ca (Test 2 only, but resolved with the new protocols – see Fig. 4*a*), and phillipsite (Z20) losing K (Fig. 4*c*). For phillipsite, only minimal 'grow-in' effects were evident in the count rate profiles for Si and Al, and then only after ~2 min.

Phillipsite (Z20) was the only test sample to display a decrease in count rate for K, but a new phenomenon of an increase in count rate for K was observed in chabazite (sbZ) (Fig. 4*b*). Indeed, the observation was repeated in a number of other chabazites (outside the present study), and their profiles have also been included in Fig. 4*b* (chabazite sbT from a Scottish vug in Tertiary basalt and chabazite IK23 from an Italian zeolitized tuff). Faujasite (fbH) additionally displayed a count rate increase for K of ~400% within the first two minutes of beam interaction, and this was accompanied by a count rate increase of ~150% for Na relative to its count rate at time = 0 (Fig. 4*c*). A perceptible increase in the count rate for Na in levyne (sbW) was also observed. Effects in the framework Al and Si count rates for all these phases are absent or extremely marginal, and the M^{2+} cations are completely unaffected under conditions for Test 4 (2 nA, 15 kV, 20 μm spot). Investigating the causes of the new observations, especially for K in chabazite, is beyond the scope of the present study but high mobilities could be associated with the large structural framework cages of chabazite and faujasite (Deer *et al.*, 2004). The crystal chemistry of phillipsite in relation to K sites and temperature is discussed in Gatta *et al.* (2009).

Test 5: Solid-solution representation and reproducibility

The principal aim in the selection of most of the reference samples was to have representation of the key 'pure' stoichiometric end-members (i.e. analcime and natrolite for Na, leucite for K, pollucite for Cs, wairakite, laumontite and goosecreekite for Ca, and edingtonite for Ba), and this has been achieved. However, as it is anticipated that many of the most useful zeolites for understanding Earth process will be found in solid-solution compositions (commonly in phillipsite, chabazite and clinoptilolite), it was considered important to develop a few of these as reference materials too. For solid solutions, compositional trends for crystal-chemical inferences are best represented

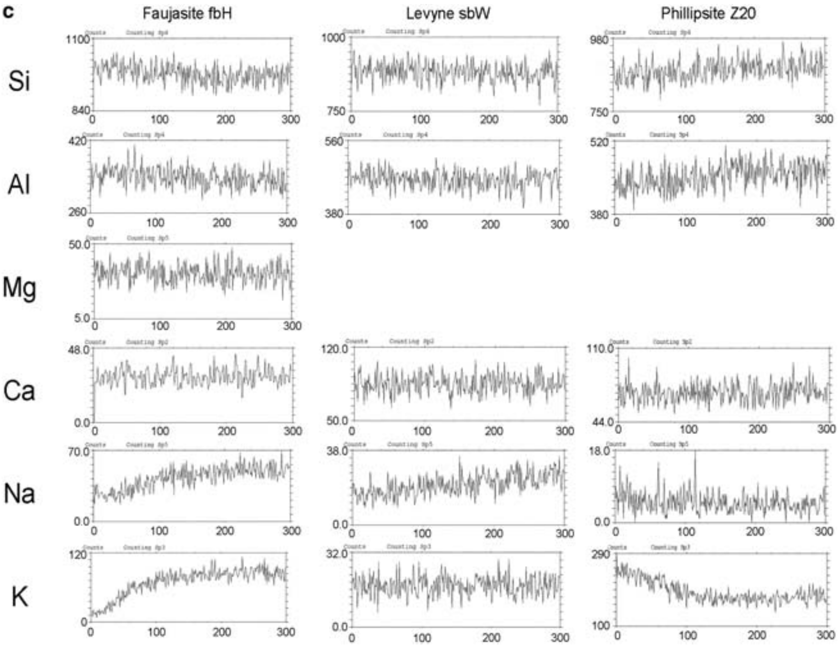

FIG. 4. Continued

graphically, so in addition to the tables of EPMA analyses (Table 4 and Supplementary file 4), ternary plots of the extra-framework cation compositions from successive batches of data have been constructed (Fig. 5). For both the levyne (sbW) and the chabazite (sbZ) in Fig. 5*a*, the data points are tightly clustered within a small range, and display no apparent differences across batches. Phillipsite (Z20) data indicate a reasonably tight compositional range across analytical-session batches, but not as tightly constrained as for levyne (sbW) and chabazite (sbZ). The X-ray maps for phillipsite (Z20) demonstrate compositional heterogeneity (chemical zoning), which partly accounts for the spread of data. Using the new data, it is observed that in levyne (sbW) and chabazite (sbZ), trends of increasing M^{2+} occur with constant Na^+/K^+ ratios, but that in phillipsite (Z20), the trend of increasing K^+ occurs with a constant Na^+/M^{2+} ratio. These observations are consistent with the crystal-chemical site preferences as detailed in Deer *et al.* (2004), and demonstrate new scope for further understanding the compositional systematics of zeolite-group minerals.

For Sr, where no end-member composition is known in nature, brewsterite from the type locality Strontian, Scotland, has provided a reasonable solid solution alternative (Fig. 5*b*). In brewsterite, the main substitutions are between Sr and Ba, but minor Na, K and Ca can be present, as seen in Supplementary file 4. Edingtonite is represented together with brewsterite in Fig. 5*b*. For Mg, faujasite from the type locality Limberg, Germany, is another complex solid-solution phase and the reference sample fbH has been characterized for similar purposes (Table 4 and Supplementary file 4). To date, only one batch of data is available for the faujasite, and the high SiO_2 content relative to reported analyses in Deer *et al.* (2004) might be indicative of minor clay contamination. Nevertheless, the data are otherwise reasonably consistent with those of Rinaldi *et al.* (1975).

Overall, these results provide confidence in inter-batch reproducibility of data where complex solid-solution compositions are anticipated.

Summary and conclusions

The reference samples

The pure compositions of Dean Quarry (UK) natrolite and analcime serve as excellent matrix blanks for all non-formula elements, including a

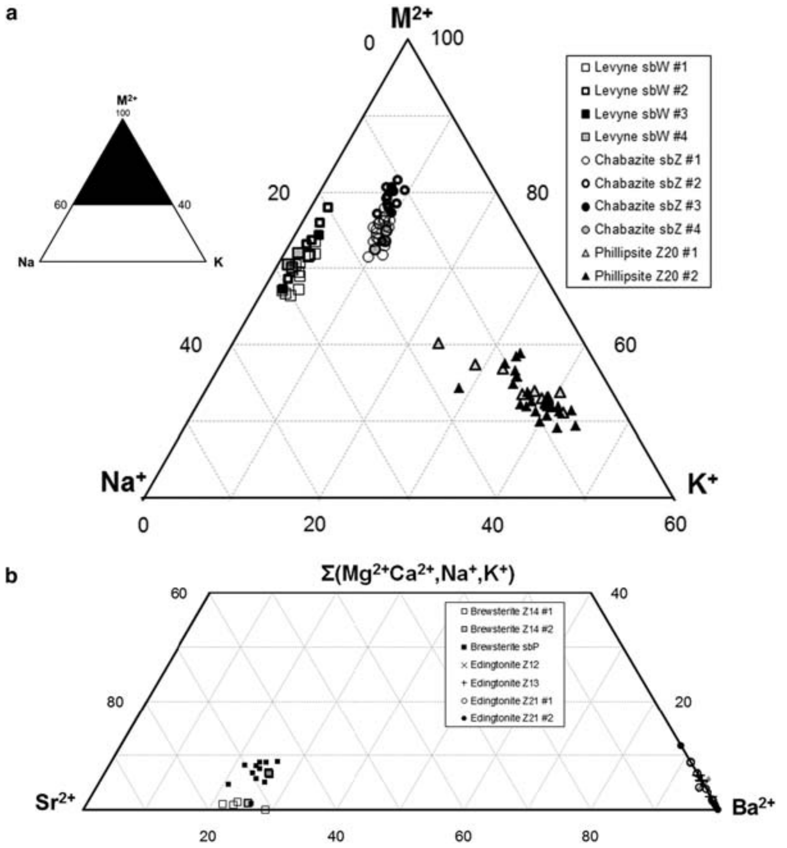

FIG. 5. Ternary representation of inter-batch reproducibility in zeolite solid-solution phases, where EC compositional ranges are expected. (*a*) Levyne, phillipsite and chabazite. (*b*) Brewsterite and edingtonite. A full set of EPMA analyses are given in Supplementary file 4.

preliminary indication at trace-element level for natrolite (fbN), as determined by LA-ICP-MS. Similarly, both the Honshu wairakite (Z17) and the Dumbartonshire edingtonite (Z12 and Z13) display high-purity compositions, except for trace Na_2O in wairakite (<0.02 wt.%) and minor K_2O in edingtonite (<0.5 wt.%). The composition of the natural Italian leucite (Z05) compares well with previous studies but a variety of elements at trace levels are reported and a small analcime component is evident. Solid-solution reference materials including brewsterite for Sr, levyne for Na-Ca, and widely occurring phillipsite and chabazite have demonstrated good inter-batch analytical reproducibility, reflecting high precision for confidence in analytical quality.

Methodology and protocols

Volatile losses have been minimized with the use of carefully selected operating conditions, but it is nevertheless recommended that responses to beam interaction are monitored with each new batch and each different mineral, by means of count-rate tests, per element, on the specified WD spectrometers. This will ensure that unexpected deviations from expected count-rate fluctuations in new samples are tracked and mitigated using the monitoring data. Monitoring is also recommended because new questions have arisen from this development work, most notably with the response of K to beam interaction in chabazite and in other specific zeolite minerals. The data processing protocol is also vitally important to ensure that only high quality analyses are accepted. Overall, the key limitations are (1) that zeolite mineral compositions involving significant Li, Be and B components cannot be adequately characterized by conventional (non-FEG) EPMA, and (2) that spatial resolution remains a challenge for many very fine-grained samples such as in zeolitized tuffs. Although there is an analytical argument that some resilient zeolites rich in M^{2+} cations might respond well with smaller spot sizes (e.g. brewsterite, laumontite), in practice, it is the common solid-solution zeolites (e.g. phillipsite, chabazite, clinoptilolite, faujasite, stilbite) that display alkali-bearing compositional variations, that are the most likely minerals to be of compositional-research interest, and that therefore also require the analytical conditions as recommended. The limitations relating to spatial resolution are not insurmountable and can be partly overcome with skilful petrographic preparations, but it is also anticipated that the advent of a new generation of microprobes (FEG technology) will allow the greatest step-change in analytical capability for zeolites.

It has been demonstrated that with careful preparations and analysis set-up conditions, the quantitative determination of major and minor elements in most of the common natural Al-Si zeolites is achievable routinely by EPMA without the need for specialist cryometric instrumentation. Robust quality-assurance procedures that include reference sample monitoring and strict data reduction criteria, are recommended as vital to the achievement of high quality analyses. Due to the complexity of solid solutions and compositional ranges in zeolite-group minerals, it is also recommended that mineral phase identification by XRD accompanies compositional studies. Stepwise recommendations for the quantitative determination of zeolite-group mineral compositions by EPMA are provided in Appendix 1.

Wider implications

With new confidence in overcoming the most challenging problems that have existed with the microbeam analysis of zeolite-group minerals, (namely, the Si-Al ratio, quantification of Na and Sr, and rationalization of the Fe issue), our protocols open new vistas for research capacity in zeolite mineralogy and Earth system sciences. Determination of zeolite-group mineral compositions will impact on understandings of volcanic-hydrothermal-diagenetic processes, alkaline fluid evolution with estimation of pressure, temperature and pH conditions, and element cycling, especially where mineral reaction paths are considered. These types of studies find application in natural resources (geochemical discrimination for mineral exploration; characterization of industrial zeolite deposits; nutrient status of volcanic soils), in natural hazards (volcanic-volatile processes that can impact on climate change), and potentially, in Earth analogue studies of Martian mineralogy.

Acknowledgements

This work was financially supported by NERC-SoS Catalyst Grant NE/L002418/1: Rare Earths in Alkaline Mineral Systems (REAMS) to Linda Campbell and David Polya (University of Manchester); by NERC-IAA-Manchester Grant 002 also to LC and DP, with the Mineral Industry Research Organisation (MIRO); and by an Erasmus Award to Linda Campbell. Reference sample donations are gratefully acknowledged (Table 3), with additional thanks to Neil Hubbard for making the skilfully curated samples of the late lsobel Geldart (British Micromount Society), available for research, and to Goldschmidt 2013 field leaders (S. Conticelli *et al.*) for assistance in collecting IK23 volcanic tuff (Vico, chabazite, Fig. 4*b*). This study benefitted from academic and technical input from J. Spratt, H. Müller-Sigmund, A. Langella, T. Weisenberger, G. Droop, K. Brodie, D. Chavrit, J. Fellowes and S. Stockley. Detailed and constructive comments of two anonymous reviewers have been welcomed, resulting in several improvements to this paper.

References

Bear, A.N., Giordano, G., Giampaolo, C. and Cas, R.A.F. (2009) Volcanological constraints on the post-emplacement zeolitisation of ignimbrites and geoarchaeological implications for Etruscan tomb construction (6th–3rd century B.C) in the Tufo Rosso a Scorie Nere, Vico Caldera, central Italy. *Journal of Volcanology and Geothermal Research*, **183**, 183–200.

Bish, D.L. and Carey, J.W. (2001) Thermal properties of natural zeolites. Pp. 403–452 in: *Natural Zeolites: Occurrence, Properties, Applications* (D. Bish and D. Ming, editors) Reviews in Mineralogy and Geochemistry, **45**. Mineralogical Society of America and Geochemical Society, Washington DC.

Bish, D.L. and Ming, D.W. (Editors) (2001) *Natural Zeolites: Occurrence, Properties, Applications*. Reviews in Mineralogy and Geochemistry, **45**. Mineralogical Society of America and Geochemical Society, Washington DC, 654 pp.

Campbell, L.S., Dyer, A., Williams, C. and Lythgoe, P.R. (2012) The masquerade of alkaline-carbonatitic tuffs by zeolites: A new global pathfinder hypothesis. *Mineralium Deposita*, **47**, 371–382.

Campbell, L.S., Dyer, A., Williams, C. and Lythgoe, P.R. (2013) Exploring the preservation of alkaline-carbonatitic extrusive rocks in relation to continent formation. *Mineralogical Magazine*, **77**, Abstract p. 814.

Campbell, L.S., Charnock, J. and Dyer, A. (2014) Regional prospecting: Can we couple large-scale exploration data with novel geochemical discrimination? [Abstracts of the 38th Annual Meeting of the Mineral Deposits Studies Group, Southampton, UK]. *Applied Earth Science: Transactions of the Institutions of Mining and Metallurgy: Section B*, **124**, 25–26.

Campbell, L.S., Charnock, J., Pearce, N.J.G. and Dyer, A. (2015) Partial proxies for geochemical discrimination in Italian altered tuffs. *Abstracts of the 51st Annual Meeting of the Volcanic and Magmatic Studies Group*, Norwich, UK, p. 53.

Cappelletti, P., Petrosino, P., de Gennaro, M., Colella, A., Graziano, S.F., D'Amore, M., Mercurio, M., Cerri, G., de Gennaro, R., Rapisardo, G. and Langella, A. (2015) The "Tufo Giallo Della Via Tiberina" (Sabatini Volcanic District, central Italy): A complex system of lithification in a pyroclastic current deposit. *Mineralogy and Petrology*, **109**, 85–101.

Cazaux, J. (2004) About the mechanisms of charging in EPMA, SEM, and ESEM with their time evolution. *Microscopy and Microanalysis*, **10**, 670–684.

Čejka, J., Corma, A. and Zones, S. (2010) *Zeolites and Catalysis: Synthesis, Reactions and Applications.* Wiley-VCH, Germany.

Chipera, S.J. and Apps, J.A. (2001) Geochemical stability of natural zeolites. Pp. 117–161 in: *Natural Zeolites: Occurrence, Properties, Applications* (D. Bish and D. Ming, editors) Reviews in Mineralogy and Geochemistry, **45**. Mineralogical Society of America and Geochemical Society, Washington DC.

Colella, C. (1996) Ion exchange equilibria in zeolite minerals. *Mineralium Deposita*, **31**, 554–562.

Dakovič, A., Trgo, M. and Langella, A. (editors) (2014) Book of Extended Abstracts. *Zeolite 2014: The 9th International Conference on the Occurrence, Properties and Utilization of Natural Zeolites.* Belgrade, Serbia, 258 pp.

Danisi, R.M., Armbruster, T. and Nagashima, M. (2015) Structural intergrowth of merlinoite/phillipsite and its temperature-dependent dehydration behaviour: a single-crystal X-ray study. *Mineralogical Magazine*, **79**, 191–203.

Deer, R.A., Howie, W.A., Wise, W.S. and Zussman, J. (2004) *Rock Forming Minerals, Volume 4B. Framework silicates: Silica Minerals, Feldspathoids and the Zeolites. 2nd edition*. The Geological Society, London, 982 pp.

Dyer, A. (1988) *An Introduction to Zeolite Molecular Sieves.* John Wiley and Sons, 149 pp.

Dyer, A. (2000) Applications of natural zeolites in the treatment of nuclear wastes and fall-out. Pp. 319–368 in: *Environmental Mineralogy: Microbial Interactions, Anthropogenic Influences, Contaminated Land and Waste Management* (J.D. Cotter-Howells, L.S. Campbell, E. Valsami-Jones and M. Batchelder (editors). Mineralogical Society Special Publication, **9**. Mineralogical Society of Great Britain and Ireland, London.

Dyer, A. (2007) Ion-exchange properties of zeolites and related materials. Pp. 525–553 in: *Introduction to Zeolite Science and Practice, 3rd Revised Edition* (J. Čejka, H. VanBekkum, A. Corma and F. Schüth, editors). Studies in Surface Science and Catalysis, **168**. Elsevier Science Bv, Amsterdam.

Dyer, A., Newton, J. and Pillinger, M. (2010) Synthesis and characterisation of mesoporous silica phases containing heteroatoms, and their cation exchange properties. Part 3. Measurement of distribution coefficients for uptake of 137-Cs, 89-Sr and 57-Co radioisotopes. *Microporous and Mesoporous Materials*, **130**, 56–62.

Eisenman, G. (1962) Cation selective glass electrodes and their mode of operation. *Biophysical Journal*, **2**, 259–323.

Fakhfakh, S., Jbara, O., Rondot, S., Hadjadj, A., Patat, J. M. and Fakhfakh, Z. (2010) Analysis of electrical charging and discharging kinetics of different glasses under electron irradiation in a scanning electron microscope. *Journal of Applied Physics*, **108**, 093705.

Fischer, R.X. (2014) Natural zeolites – a treasure in zeolite science. (Invited contribution). *Zeolite 2014. The 9th International Conference on the Occurrence, Properties, and Utilization of Natural Zeolites, Belgrade, Serbia.* Book of Abstracts, 11.

Gatta, G.D., Rotiroti, N., Bellatreccia, F. and Della Ventura, G. (2007) Crystal chemistry of leucite from the Roman Comagmatic Province (central Italy): A multi-methodological study. *Mineralogical Magazine*, **71**, 671–682.

Gatta, G.D., Cappelletti, P., Rotiroti, N., Slebodnick, C. and Rinaldi, R. (2009) New insights into the crystal structure and crystal chemistry of the zeolite phillipsite. *American Mineralogist*, **94**, 190–199.

Giampaolo, C. and Lombardi, G. (1994) Thermal-behavior of analcimes from 2 different genetic environments. *European Journal of Mineralogy*, **6**, 285–289.

Giampaolo, C., Godano, R.F., DiSabatino, B. and Barrese, E. (1997) The alteration of leucite-bearing rocks: A possible mechanism. *European Journal of Mineralogy*, **9**, 1277–1291.

Giampaolo, C., Lo Mastro, S., De Rita D., Giordano, G. (2008) Lateral and vertical zeolite grade variations in the Tufo Lionato ignimbrite unit (Colli Albani, Roma, Central Italy). *Zeolite '06: The 7th International Conference of the Occurrence, Properties and Utilization of Natural Zeolites, Socorro, New Mexico, USA*. Book of Abstracts, 119–120.

Harjula, R., Lehto, J., Pothuis, J.H., Dyer, A. and Townsend, R.P. (1993) Ion-exchange in zeolites. 2. Hydrolysis and dissolution of zeolites NaX and NaY. *Journal of the Chemical Society – Faraday Transactions*, **89**, 971–976.

Hay, R.L. and Sheppard, R.A. (2001) Occurrence of zeolites in sedimentary rocks: An overview. Pp. 217–234 in: *Natural Zeolites: Occurrence, Properties, Applications* (D. Bish and D. Ming, editors) Reviews in Mineralogy and Geochemistry, **45**. Mineralogical Society of America and Geochemical Society, Washington DC.

Heister, L.E., O'Day, P.A., Brooks, C.K., Neuhoff, P.S. and Bird, D.K. (2001) Pyroclastic deposits within the East Greenland Tertiary flood basalts. *Journal of the Geological Society*, **158**, 269–284.

Henderson, C.M.B., Bell, A.M.T., Kohn, S.C. and Page, C.S. (1998) Leucite-pollucite structure-type variability and the structure of a synthetic end-member calcium wairakite ($CaA1_2Si_4O_{12}.2H_2O$). *Mineralogical Magazine*, **62**, 165–178.

Henderson, C.M.B., Hamilton, D.L. and Waters, J.P. (2014) Phase equilibria in $NaAlSiO_4$–$KAlSiO_4$–SiO_2–H_2O at 100 MPa pressure: Equilibrium leucite composition and the enigma of primary analcime in blairmorites revisited. *Mineralogical Magazine*, **78**, 171–202.

Kearns, S. and Buse, B. (2012) X-ray microanalysis of volcanic ash. *IOP Conference Series: Materials Science and Engineering*, **32**, Abstract 012013.

Kim, E., Lee, T., Kim, H., Jung, W.-J., Han, D.-Y., Baik, H., Choi, N. and Choi, J. (2014) Chemical vapor deposition on chabazite (CHA) zeolite membranes for effective post-combustion CO_2 capture. *Environmental Science & Technology*, **48**, 14828–14836.

Langella, A., Cappelletti, P. and de'Gennaro, R. (2001) Zeolites in closed hydrologic systems. Pp. 235–260. in: *Natural Zeolites: Occurrence, Properties, Applications* (D. Bish and D. Ming, editors) Reviews in Mineralogy and Geochemistry, **45**. Mineralogical Society of America and Geochemical Society, Washington DC.

Langella, A., Bish, D.L., Cappelletti, P., Cerri, G., Colella, A., de Gennaro, R., Graziano, S.F., Perrotta, A., Scarpati, C. and de Gennaro, M. (2013) New insights into the mineralogical facies distribution of Campanian Ignimbrite, a relevant Italian industrial material. *Applied Clay Science*, **72**, 55–73.

Line, C.M.B., Putnis, A., Putnis, C. and Giampaolo, C. (1995) The dehydration kinetics and microtexture of analcime from 2 parageneses. *American Mineralogist*, **80**, 268–279.

Merlet, C. and Llovet, X. (2012) Uncertainty and capability of quantitative EPMA at low voltage – A review. *Materials Science and Engineering*, **32**, Abstract 012016.

Morgan, G. and London, D. (1996) Optimizing the electron microprobe analysis of hydrous alkali aluminosilicate glasses. *American Mineralogist*, **81**, 1176–1185.

Morgan, G.B. and London, D. (2005) Effect of current density on the electron microprobe analysis of alkali aluminosilicate glasses. *American Mineralogist*, **90**, 1131–1138.

Neuhoff, P.S. and Ruhl, L.S. (2006) Mechanisms and geochemical significance of Si-Al substitution in zeolite solid solutions. *Chemical Geology*, **225**, 373–387.

Neuhoff, P.S., Fridriksson, Th. and Bird, D.K. (2000) Zeolite parageneses in the North Atlantic Igneous Province: Implications for geotectonics and groundwater quality of basaltic crust. *International Geology Review*, **42**, 15–44. Reprinted in: Frontiers in Geochemistry: Global Inorganic Geochemistry (Konrad Krauskopf Volume 1) (W.G. Ernst, editor). *Geological Society of America, International Book Series*, **5**, 271–300.

Passaglia, E. (1970) Crystal chemistry of chabazites. *American Mineralogist*, **55**, 1278–1301.

Passaglia, E. and Sheppard, R.A. (2001) The crystal chemistry of zeolites. Pp. 69–116 in: *Natural Zeolites: Occurrence, Properties, Applications* (D. Bish and D. Ming, editors) Reviews in Mineralogy and Geochemistry, **45**. Mineralogical Society of America and Geochemical Society, Washington DC.

Passaglia, E., Vezzalini, G. and Carnevali, R. (1990) Diagenetic chabazites and phillipsites in Italy – crystal-chemistry and genesis. *European Journal of Mineralogy*, **2**, 827–839.

Pearce, N.J.G., Abbott, P.M. and Martin-Jones, C. (2014) Microbeam methods for the analysis of glass in fine-grained tephra deposits: A smart perspective on current and future trends. *Marine Tephrochronology*, **398**, 29–46.

Pekov, I.V., Turchkova, A.G., Chukanov, N.V., Zadov, A. E. and Grishin, B.G. (2000) Chabazite-Sr (SrCa) $[Al_2Si_4O_{12}]\cdot 6H_2O$ – A new zeolite from the Lovozero Massif, Kola peninsula. *Zapiski Vserossiyskogo Mineralogicheskogo Obshchestva*, **129**, 52–58.

Pham, T.D., Hudson, M.R., Brown, C.M. and Lobo, R.F. (2014) Molecular basis for the high CO_2 adsorption capacity of chabazite zeolites. *Chemsuschem*, **7**, 3031–3038.

Putnis, C.V., Geisler, T., Schmid-Beurmann, P., Stephan, T. and Giampaolo, C. (2007) An experimental study of the replacement of leucite by analcime. *American Mineralogist*, **92**, 19–26.

Rigby, M., Droop, G., Plant, D. and Graser, P. (2008) Electron probe micro-analysis of oxygen in cordierite: Potential implications for the analysis of volatiles in minerals. *South African Journal of Geology*, **111**, 239–250.

Rinaldi, R., Smith, J.V. and Jung, G. (1975) Chemistry and paragenesis of faujasite, phillipsite and offretite from Sasbach, Kaiserstuhl, Germany. *Neues Jahrbuch für Mineralogie: Abhandlungen*, 433–443.

Saunders, K., Buse, B., Kilburn, M.R., Kearns, S. and Blundy, J. (2014) Nanoscale characterisation of crystal zoning. *Chemical Geology*, **364**, 20–32.

Utada, M. (2001) Zeolites in hydrothermally altered rocks. Pp. 305–322 in: *Natural Zeolites: Occurrence, Properties, Applications* (D. Bish and D. Ming, editors) Reviews in Mineralogy and Geochemistry, **45**. Mineralogical Society of America and Geochemical Society, Washington DC.

Vaggelli, G., Olmi, F. and Conticelli, S. (1999) Quantitative electron microprobe analyses of reference silicate mineral and glass samples. *Acta Vulcanologica*, **11**, 297–303.

Vignaroli, G., Aldega, L., Balsamo, F., Billi, A., De Benedetti, A., De Filippis, L., Giordano, G. and Rossetti, F. (2014) A way to hydrothermal paroxysm, Colli Albani Volcano, Italy. *Geological Society of America Bulletin*, B31139.

Wallace, S.H., Shaw, S., Morris, K., Small, J.S. and Burke, I.T. (2013) Alteration of sediments by hyperalkaline K-rich cement leachate: Implications for strontium adsorption and incorporation. *Environmental Science & Technology*, **47**, 3694–3700.

Wang, H.W. and Bish, D.L. (2012) Infrared spectroscopic characterization of dehydration and accompanying phase transition behaviors in NAT-topology zeolites. *Physics and Chemistry of Minerals*, **39**, 277–293.

Wang, H.W. and Bish, D.L. (2014) Host-guest interactions in zeolites: Insights from the NAT-topology system. *Zeolite 2014. The 9th International Conference on the Occurrence, Properties, and Utilization of Natural Zeolites, Belgrade, Serbia.* Book of Abstracts, 239–240.

Weisenberger, T. and Spürgin, S. (2009) Zeolites in alkaline rocks of the Kaiserstuhl Volcanic Complex, SW Germany – new microprobe investigation and the relationship of zeolite mineralogy to the host rock. *Geologica Belgica*, **12**, 75–91.

Weisenberger, T.B., Rahn, M., van der Lelij, R., Spikings, R.A. and Bucher, K. (2012) Timing of low-temperature mineral formation during exhumation and cooling in the Central Alps, Switzerland. *Earth and Planetary Science Letters*, **327**, 1–8.

Weisenberger, T.B., Spürgin, S. and Lahaye, Y. (2014) Hydrothermal alteration and zeolitization of the Fohberg phonolite, Kaiserstuhl Volcanic Complex, Germany. *International Journal of Earth Sciences*, **103**, 2273–2300.

APPENDIX 1: RECOMMENDED PROTOCOLS

1. *Microprobe Analysis Protocol*
    1.1. Where sample sections have been pre-examined by electron beam methods (e.g. SEM, cathodoluminescence microscopy), a short re-polish at the finest grade should be considered prior to EPMA, to refresh the mineral surface (on the scale of a few micrometres, or equivalent to the beam penetration depth), for mitigation of any previous effects of alkali migration.
    1.2. Carbon-coat freshly polished samples and reference blocks.
    1.3. Undertake routine instrument calibration procedures.
    1.4. Set up the analysis declaration, with suggested conditions of 2 nA, 15 kV and a 20 μm defocused beam, shown to work well for non-FEG EPMA. For all zeolite minerals, cation oxides can be output on an anhydrous basis, but with H_2O accounted for in the ZAF corrections. Cation oxides can then be normalized to 24 oxygens (recalculated later according to the specific mineral phase analysed), and the H_2O component returned by difference from 100% using the total oxide wt.%. Iron should be included as Fe_2O_3. It is vital that all available spectrometers are utilized for the simultaneous detection of the most susceptible elements first; Na, Al and K, and if possible, Si too. In our set-up, Si had to follow Al on spectrometer 4, as only two TAP crystal detectors were available, the other one on spectrometer 5 being needed for Na detection first, followed by Mg. For the LIF detector on spectrometer 1, Cs as a group I alkali metal had priority over Fe, and for the two PET detectors, K and Ca were determined first, followed by Sr and Ba. A general guide is that the alkalis and lightest elements are potentially the most mobile under the electron beam.

1.5. Conduct count-rate monitoring tests on the phase(s) to be analysed, per element, per spectrometer, according to the spectrometer configuration in the analysis declaration (for this study, see Table 1 and Fig. 4). This is only necessary once per sample.

1.6. Analyse reference zeolites appropriate to the expected sample compositions with each new session. A minimum of five replicate analyses is recommended for pure 'end-member' compositions (e.g. natrolite, edingtonite), and significantly more for solid-solution references (e.g. phillipsite, brewsterite).

1.7. Sample points: For samples where spatial resolution and/or polish quality is not an issue (hydrothermal, cavity types), it is expected that at least 90% of the data will be acceptable after data processing, so the number of replicate analyses required can be reasonably estimated. For challenging samples (volcanic tuffs, saline lake deposits, acicular clusters and others where petrographic examination has revealed potential sub-surface inclusions or intergrown phases), the quantity of usable data might be as low as 20% (or even non-achievable due to fine grained textures and/or persistent subsurface non-zeolite phases such as smectite clays, oxides or precursor glass), so larger numbers of analysis points need to be planned. In such circumstances, investment of time in skilful petrographic preparation becomes especially worthwhile.

2. *Data Reduction and Quality Control Protocol*

2.1. Make a preliminary calculation of total oxides by wt.%, and of Si:Al using the conventional T_{Si} or '*R*' value: Si/(Si + Al) for most zeolites. For leucite and other phases where tetrahedral Fe^{3+} is indicated, Si/(Si + Al + Fe) should be used, but with care, due to potential contamination from Fe-oxide phases. Refrain from evaluating the calculated total oxides at this stage.

2.2. Calculate the charge balance, *E*%, according to Passaglia (1970) and Deer *et al.* (2004): $E\% = 100 \times [(Al + Fe^{3+}) - (\Sigma M^{+}) - 2(\Sigma M^{2+})]/[(\Sigma M^{+}) + 2(\Sigma M^{2+})]$, where M^{+} represents alkali cations and M^{2+} represents alkaline earths. Again, refrain from evaluating the results at this stage.

2.3. Next, determine the presence of contaminants, using $Fe_2O_3 > 0.2$ wt.% as a guide, and optionally, $P_2O_5 >$ LOD (limit of detection). For most zeolites other than faujasite, high MgO is also a suspicious indicator due to the potential presence of smectite clay minerals, ideally avoided with careful petrographic preparations. Where the *R* value and *E*% are sound, minor MgO is acceptable in the analysis. Delete the contaminant-specific components (mainly Fe_2O_3) from the analyses.

2.4. Recalculate total anhydrous oxides, *E*% and *R*.

2.5. At this stage, apply the criteria of *E*% and *R* range limitations to the data, omitting analyses with *E*% less than –10 or greater than +10, and *R* values outside the mineral-specific ranges specified in table 1 of Passaglia and Sheppard (2001).

2.6. Omit further data that lie outside the range of total non-volatile oxides of between 80–95 wt.%, except for leucite (anhydrous, ideally 100%). Optionally, accept totals lower than 80 wt.%.

2.7. Next, acceptable analyses can be processed for limits of detection, determined per oxide, per mineral, per session from the average listings of the element 1-sigma data, recalculated to oxide 3-sigma values. All data components below these limits of detection are deleted, and the quality parameters of total anhydrous oxides, *R* and *E*% again recalculated.

2.8. The H_2O component can now be estimated on the basis of 100–(total oxides)%.

2.9. Calculation of mineral formulae is undertaken according to the conventions set out in Deer *et al.* (2004) based on numbers of framework oxygen atoms specific to each different mineral species. Using cation proportions that were determined on the basis of 24 oxygens, and omitting all the non-formula and sub-detection components as above, re-normalize according to the mineral phase in question, i.e. 24 oxygens for chabazite, 20 for edingtonite, 96 for analcime, etc.

2.10. Calculate the sums of the framework tetrahedral components and the extra-framework cation components, respectively.